Enhancement of deuteron-fusion reactions in metals and experimental implications

A. Huke,[1,*] K. Czerski,[1,2] P. Heide,[1] G. Ruprecht,[1,3] N. Targosz,[2] and W. Żebrowski[2]

[1]*Institut für Optik und Atomare Physik, Technische Universität Berlin, Hardenbergstraße 36, D-10623 Berlin, Germany*

[2]*Institute of Physics, University of Szczecin, Szczecin, Poland*

[3]*TRIUMF, Vancouver, British Columbia, Canada*

(Received 23 April 2007; revised manuscript received 28 April 2008; published 21 July 2008)

Recent measurements of the reaction ^{2}H$(d, p)^3$H in metallic environments at very low energies performed by different experimental groups point to an enhanced electron screening effect. However, the resulting screening energies differ strongly for diverse host metals and different experiments. Here, we present new experimental results and investigations of interfering processes in the irradiated targets. These measurements inside metals set special challenges and pitfalls that make them and the data analysis particularly error prone. There are multiparameter collateral effects that are crucial for the correct interpretation of the observed experimental yields. They mainly originate from target surface contaminations owing to residual gases in the vacuum as well as from inhomogeneities and instabilities in the deuteron density distribution in the targets. To address these problems an improved differential analysis method beyond the standard procedures has been implemented. Profound scrutiny of the other experiments demonstrates that the observed unusual changes in the reaction yields are mainly due to deuteron density dynamics simulating the alleged screening energy values. The experimental results are compared with different theoretical models of the electron screening in metals. The Debye-Hückel model that has been previously proposed to explain the influence of the electron screening on both nuclear reactions and radioactive decays can be clearly excluded.

DOI: 10.1103/PhysRevC.78.015803 PACS number(s): 25.45.−z, 25.60.Pj, 26.20.−f, 23.90.+w

I. INTRODUCTION

The cross section for nuclear reactions between charged particles at low energies is mainly determined by the penetration probability through the Coulomb barrier, which results in a steep exponential decrease toward lower energies. At sufficiently low energies, however, this decrease is slowed down by screening the Coulomb barrier by the inevitable presence of surrounding electrons. The electron screening was originally taken into account for nuclear reactions proceeding in dense astrophysical plasmas in the interior of stars [1] where the nuclear reaction rates can be increased even by many orders of magnitude. For laboratory investigations of nuclear reactions at very low energies, this effect was theoretically described [2] and experimentally observed in different fusion reactions on gas targets (e.g., Ref. [3]). The corresponding enhancement of the nuclear cross section could be explained by the gain of electron binding energies between the initial distant atoms and the final fused atom. This was attributed to the rise of the kinetic energy of colliding nuclei and was termed the electron screening energy. Electron screening resulting from free electrons, which are much more important for astrophysical applications, was first investigated in the $d+d$ fusion reactions taking place in metallic environments [4–6]. The experimentally determined screening energies for some heavier metals were one order of magnitude larger than the gas target value [7] and larger by a factor of about 4 than the theoretical predictions [8]. These experimental results were also confirmed by other authors [9–14].

Meanwhile, the electron screening effect in $d+d$ fusion reactions has been studied for over 50 different metals and some insulators [12–14], allowing, in principle, for a systematic study of the target material dependence of the electron screening energy. Unfortunately, there are some discrepancies among experimental values obtained by different groups [15]. These probably arise from some experimental systematic uncertainties connected with oxidation of the target surface or with a high mobility of the implanted deuterons under beam irradiation, which can lead to unstable deuteron density profiles within the target. Both effects play a crucial role in the experimental determination of the screening energies [6,16]. The basic quantity received from the experiment is the nuclear reaction yield, which is given for a thick target as an integral over the range of the projectiles $Y = \int_0^R [n\sigma]\, dx$ for a target nuclei density distribution n and cross section σ. So deviations in the observed yield have two principal causes: changes in the deuteron density profile and modification of the cross section, probably by the screening effect, which are merged in the integrant product $[n\sigma]$. Some standard experimental difficulties have been already discussed in our antecedent paper [16], where an especially adapted data acquisition and analysis method, allowing us to discern between changes in n and σ, has been presented in a systematic manner. Based on this method, we report here some new experimental results and estimate experimental uncertainties of previous experiments. We additionally compare data obtained by different groups and discuss systematic errors of applied experimental and analytical methods.

From the theoretical point of view, the large number of experimental data corrected for the discussed experimental uncertainties enables a comparison with theoretical predictions. The first *ab initio* quantum mechanical calculation of the screening energy in a crystal environment has been recently performed by using realistic wave functions [17]. However,

*huke@physik.tu-berlin.de, Armin.Huke@web.de

the results are still unsatisfying because of the very high demand for computational power, limiting the model accuracy. Thus, the self-consistent dielectric function theory developed previously [18] will be used here for the calculation of the screening energy contributions coming not only from free electrons but also from bound electrons of reacting nuclei and host metals. Additionally, the interaction with the crystal lattice will be included. The theoretical results will be extended for comparison with the last experimental studies of the electron screening in nuclear reactions between heavier nuclei [19–21] and in radioactive decays [22–24]. However, it has recently been suggested that the enhanced electron screening can be explained within the classical Debye-Hückel model [13]. The idea has been supported by an observation of the predicted inverse proportionality of the experimental screening energies to the square root of the absolute target temperature [25,26]. As a consequence one could expect a magnification of the α and β^+ decay rates when radioactive sources are put in metals at cryogenic temperatures. Even though the Debye screening cannot be applied to strongly coupled electron plasmas, as metals at moderate temperatures are, the suggestion has generated much interest [23,27–29]. Thus, both experimental and theoretical aspects of the temperature effect of the electron screening will be the subject of a critical discussion clearly showing the inapplicability of the Debye-Hückel model for these issues.

II. EXPERIMENTAL SETUP, DATA ACQUISITION, AND ANALYSIS

The experiments have been carried out at an accelerator optimized for low-energy beams. Figure 1 illustrates the principal setup and the data acquisition system. The accelerator consists of a radio frequency ion source, an acceleration line powered by a highly stabilized 60-kV supply, and subsequent electric quadrupoles for focusing and a magnetic dipole for beam analysis. The beam impinges onto a Faraday cup just inside the target chamber, where beam adjustment can be done without disturbing the deuteron density in the targets. A horizontal magnetic steerer is used to deflect the beam onto the target, thus removing neutral particles and contaminations carried along by the beam. A cylinder box set to a negative potential surrounds the target to suppress secondary electrons. The isolated target holder is connected to a current integrator. The targets were disks made from different pure metals, becoming self-implanted deuterium targets under the beam irradiation. Four Si detectors at laboratory angles of 90°, 110°, 130°, and 150° were used for the detection of all charged particles: p,^{3}H, and ^{3}He of the reactions ^{2}H$(d, p)^3$H and ^{2}H$(d, n)^3$He. The detectors needed to be shielded from the backscattered deuterons to prevent a congestion of them in the data acquisition system. Therefore grounded Al foils of thicknesses from 120 to 150 $\mu g/\text{cm}^2$ were placed in front of the detectors. The thickness is sufficient to block deuterons up to 60 keV while all other ejectiles could pass. The detector voltage pulses travel through preamplifiers and spectroscopic amplifiers. The signals are digitized by four ADCs in an embedded VME system connected to a computer, which automatically integrates the proton lines of the spectra in fixed time intervals[1] and records the four differential counting numbers $N(\theta)$ and the charge q of the integrated beam current at the target in a file, which then can be further processed. An

[1]The time intervals are $\geqslant$10 s limited by the serial line.

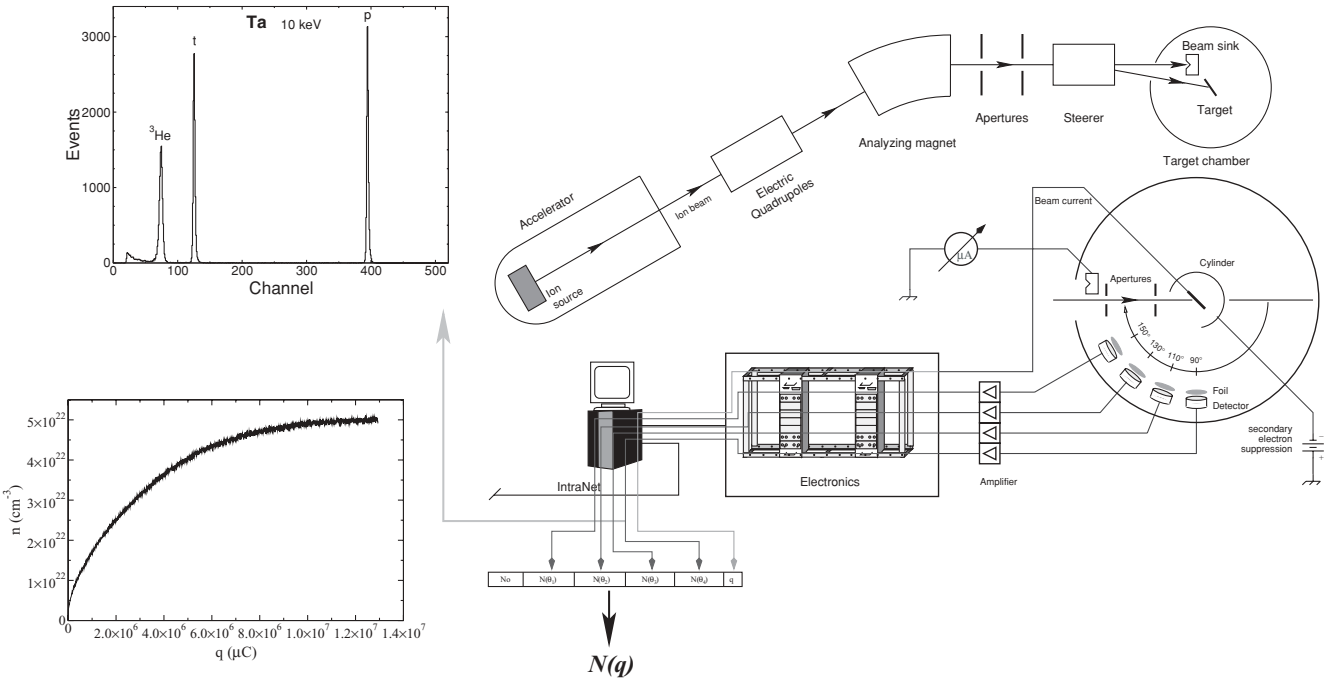

FIG. 1. Experimental setup.

example spectrum is shown in Fig 1; all ejectile lines are clearly identifiable. Owing to the anisotropic angular distribution of the ejectiles of the $d+d$ fusion reactions even at the lowest energies, a total counting number N is calculated by providing the tabulated function $N(q)$, which is the basic quantity for the further data analysis.

Correspondingly, the experimental reaction yield is given by

$$Y(E) = \frac{ze}{\varepsilon}\frac{dN}{dq}, \tag{1}$$

where the number of impacting projectiles is already substituted by their charge, ε is the detector efficiency, and z the charge state of the projectile. The yield can be calculated for an infinitely thick target (with regard to the projectile range R) by

$$Y_{\text{theory}}(E) = \int_0^R n \cdot \sigma\,[E(x)]\,dx, \tag{2}$$

where the number density of the target nuclei is n and the cross section is σ. Unlike other chemical compounds the small hydrogen atoms are not trapped in firm chemical bonds with metals. The hydrogen density is not bound to a fixed stoichiometric ratio and can and indeed does change under ion irradiation. Changes in the yield may now originate from both the deuteron density and the cross section and need to be discriminated. The density is here a function of the target depth, the projectile energy, the implanted charge, the beam flux, and other target-material-dependent and environmental conditions. The tabulated function $N(q)$ provided by our data acquisition system makes it possible to retain the differentiation in Eq. (1) and thereby gain information on the charge development of a depth-averaged density $n(q)$. So by assuming depth homogeneity of the deuteron density in Eq. (2) the depth x can be substituted by the projectile energy E with the stopping power differential equation [30]

$$\frac{dE}{dx} = -\left(c_M + \frac{n(q)}{n_D}c_D\right)\sqrt{E}, \tag{3}$$

where c_M and c_D are the stopping power coefficients in the metal and in hydrogen, respectively, and n_D is the appendant hydrogen density. Applying this substitution one arrives at a motivation and an expression for the *reduced yield* [5,6,16]

$$y(E;q) := \frac{Y(E;q)}{\int_0^E \frac{\sigma(E)}{\sqrt{E}}dE} = \frac{n(q)}{c_M + \frac{n(q)}{n_D}c_D} \times F(E). \tag{4}$$

Since both the cross section in the metallic environment and the deuteron density are unknown the yield needs to be set in relation to a known gas target cross section. We therefore chose the parametrization from Ref. [31] because it has the highest precision. It forms together with the low-energy function ($\sqrt{E}$) of the stopping power [Eq. (3)] the integral in the denominator on the right-hand side. The expression printed in gray is *per se* a constant. So if the reduced yield is not constant it is based on deviations of the prescribed progression in the cross section or in the functional dependence of the stopping powers or changes in the density. It is a sensitive measure for such deviations but the distinction of the possible reasons is a matter of reasonable interpretation. Figure 2 shows plots of the reduced yield at two different energies.

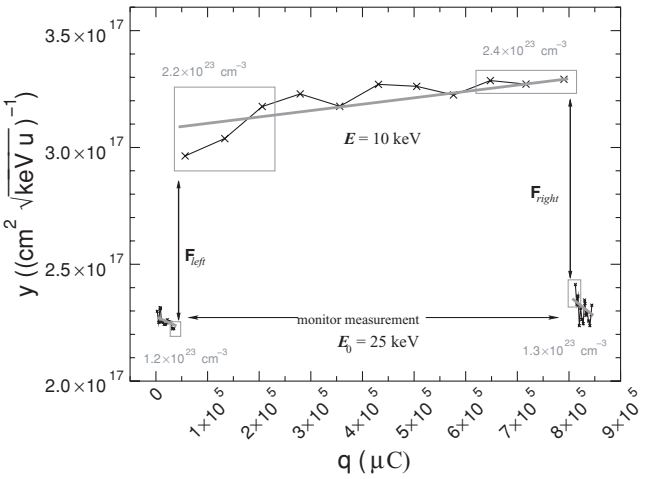

FIG. 2. Analysis procedure at the example of zirconium at 10 keV.

One can see long-term changes in the individual measurements indicated by the straight lines. These are attributed to changes in the deuteron density profiles scattered by the counting statistics, of course. In contrast, the large discontinuities of the reduced yield at the switching of the beam energy result from a modification of the cross section. This is taken into account by the enhancement factor $F(E)$ in Eq. (4). Since the absolute quantity of the deuteron density is unknown for the practical analysis a normalized enhancement factor is defined as

$$F_{\text{norm}}(E) := \frac{y(E)}{y(E_0)} = \frac{F(E)}{F(E_0)}, \tag{5}$$

with the normalization energy E_0 chosen to be 25 keV for the monitor measurements. The gray rectangles indicate the points from which the experimental error for F_{norm} is inferred. Thus not only errors from the counting statistics but also from long-term changes of the density are included. Results obtained for different projectile energies are displayed in Fig. 3.

Assuming electron screening as the reason for the increase of F_{norm} and adopting U_e as a kinetic energy shift parameter called the screening energy in the cross section [2] of the yield

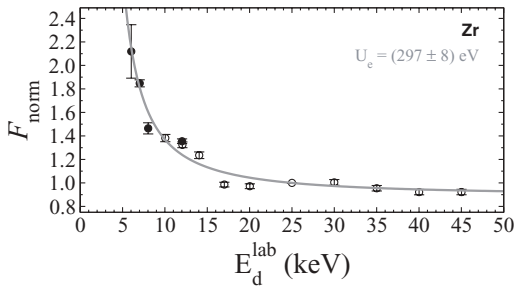

FIG. 3. Exemplary results for the enhancement factor F_{norm} showing screening enhancement for Zr theoretically described by the curve with the single parameter U_e.

one obtains [5,6,16]

$$F(E) = \frac{\int_0^E \frac{\sigma(E+2U_e)}{\sqrt{E}} dE}{\int_0^E \frac{\sigma(E)}{\sqrt{E}} dE} \tag{6}$$

for the screening enhancement factor of thick target yields.[2] The factor 2 arises from the c.m.-laboratory transformation. So F is an enhancement factor for thick targets in analogy to the enhancement factor for thin targets from Ref. [2]:

$$\begin{aligned} f(E_{\text{c.m.}}) &:= \frac{\sigma(E_{\text{c.m.}} + U_e)}{\sigma(E_{\text{c.m.}})} \\ &= \frac{\frac{1}{E_{\text{c.m.}}+U_e} S(E_{\text{c.m.}} + U_e) e^{-2\pi\eta(E_{\text{c.m.}}+U_e)}}{\frac{1}{E_{\text{c.m.}}} S(E_{\text{c.m.}}) e^{-2\pi\eta(E_{\text{c.m.}})}} \\ &\simeq e^{(\pi\eta(E_{\text{c.m.}})\frac{U_e}{E_{\text{c.m.}}})}, \quad U_e \ll E_{\text{c.m.}}, \end{aligned} \tag{7}$$

where we have used the S-factor parametrization of the cross section with the Sommerfeld parameter η in the second line and applied an approximation in the third line, which demonstrates its qualitative behavior as a roughly exponential increase for decreasing energies. The corresponding curve in Fig. 3 obtained for a fitted value of U_e supports the screening hypothesis. Our data analysis procedure is thus independent of the absolute value of the deuteron densities inside the targets and the stopping power coefficients, which otherwise would introduce errors of 10%–20%. The functional dependency of the stopping powers on the energy $\sqrt{E}$ has been repeatedly confirmed (see Ref. [32] and references therein). The reduced yield can be used to calculate a deuteron density estimate by solving Eq. (4) for $n(q)$ and supposing $F = 1$ [16, Eq. (10)]. Only for this purpose the stopping power coefficients are explicitly required. A corresponding density plot for an initial implantation in Al is shown in Fig. 1. The numbers above the gray boxes in Fig. 2 are density estimates for these areas.

This is in brief the basic experimental procedure as of Refs. [5,6,16]. For the study of the electron screening effect two experimental campaigns were executed. Since the special physicochemical properties of the hydrogen compounds and the beam-induced chemical reactions at the target heavily influence the obtained results [6,16], the second more extensive campaign needed to investigate these interfering effects ([16] Sec. 4). These are sketched in a concise survey in the next section.

III. EXPERIMENTAL SPECIALTIES AND PITFALLS

The investigation of nuclear reaction cross sections on deuterium in metals should be performed at the lowest possible energies. This means that the composition of the topmost atomic layers of the metallic target is of crucial importance because of the quickly decreasing range of the beam ions, considerably below 1 μm. This situation is unusual for experimental nuclear physics. The usual setups in experimental nuclear physics are constructed in high vacuum technology. But here the contained water vapor from the surfaces of all materials leads under ion impact to a progressive oxidation of the target metal because of the stronger electron negativity of oxygen in comparison to hydrogen. Hence, hydrogen is contained in metal oxides only in segregation at low and unstable densities. Consequently, the oxidation diminishes and eventually destroys the screening effect with the growing thickness of the metal oxide layer. Carbon hydrides contained in HV systems pose another problem, leading to carbon layers on the target as will be discussed in the following. In such a way generated alterations in the depth profile of the deuteron density distribution in the target becomes the singular dominating error source for the observed enhancement and the inferred screening energies. Our vacuum system is made of aluminium with elastomer gaskets pumped by turbo molecular pumps with auxiliary oil-lubricated two-stage rotary vane pumps and liquid N_2 cooled cryogenic traps [16], Fig. 1. A residual gas analyzer (RGA) was used to monitor the composition of the residual gas in the vacuum. This is here merely a concise presentation; for a more extensive description see Ref. [16].

In accordance to the literature about HV systems the main constituent of the residual gas is water. Because of its extraordinarily high dipole moment water vapor is very adhesive to solids and is hence chemisorbed to surfaces. Under ion irradiation several processes are enabled. Via heating and phonon excitation at the surface the beam provides the activation energy for dissociative chemisorption of the water molecule (i.e., the protons are split off and the remaining oxygen radical forms a chemical bond to the metal atoms). Essentially, the same process happens by direct impact excitation of the water molecule by the ions. The hydrogen implantation into the metal causes, aside from the usual surface deterioration, an in-depth destruction of the crystal integrity of the material known as embrittlement, which always occurs if the hydrogen loading rate is too high and not proceeding in thermal equilibrium [33]. Thus, the surface is fractalized and the oxidation can progress into the bulk of the metal, quickly creating a thick metal oxide layer. Figure 4 shows as an example a picture of the surface of an Al target that turned into a sponge-like structure.

The rate of the oxidation process depends on the concrete form of the mutual interaction potential between the water molecule and the surface atoms, establishing a material dependency. The energy supply of the beam enables these processes even for the noble metals. In general, more reactive metals are more prone to oxidation and embrittlement whereas for the embrittlement the structural difference between the metal and the metal hydride is more important. Aside from the overall beam heating the energy of the projectiles is also important because lower energy projectiles are more effective at the surface [34]. The partial pressure of water in HV is so high that there are ample supplies for the surface chemical reactions. The hit rate of water molecules with a sticking coefficient of almost one is comparable over orders of magnitude at usual beam currents of 10–100 μA. This implies a dependence on the ion flux, too. There are two counteracting processes: sputtering and thermal or ion

[2]The screening energy U_e should only be applied to the Coulomb barrier penetration in σ; see Refs. [16,18]. The correction only becomes important for far lower beam energies.

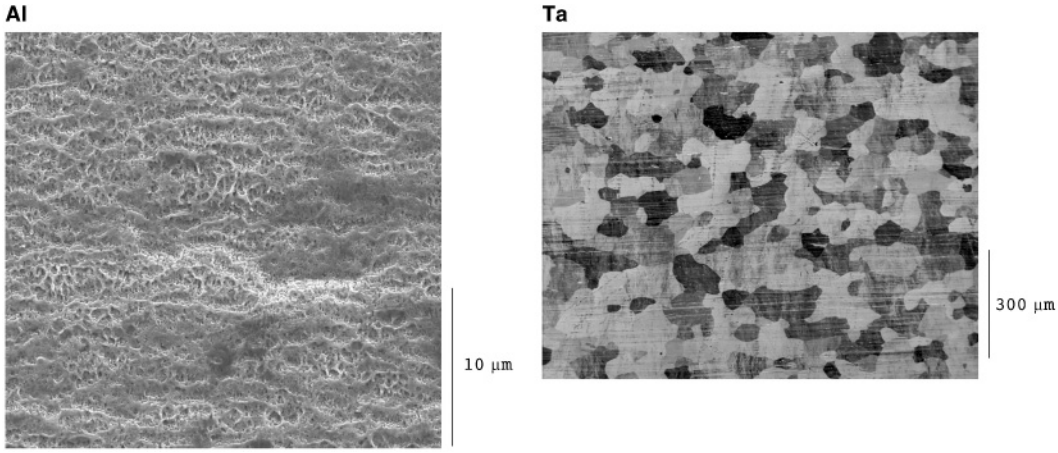

FIG. 4. Scanning electron microscopic pictures of target surfaces. Left: Symptoms of embrittlement for Al. Right: Beginning layer formation for Ta in island growth mode.

stimulated desorption. The sputtering yield of the lightweight deuterons is far too low to keep the surface clean with the resulting sputtering rate. One would expect that an increased temperature of the surface would increase the desorption rate of the water molecules. If the activation energy barrier for dissociative chemisorption of water is positive an increased temperature proliferates the oxidation.[3] The situation is similar for ion stimulated desorption/chemisorption, which again depends on the interaction potential, but usually oxidation prevails. Unless ultra high vacuum (UHV) systems equipped for entire baking are used the oxidation cannot be avoided. A deuteron irradiation of only 1 *coulomb* is enough to produce a considerable metal oxide layer (see Ref. [16] Fig. 6). There is, however, a process that is nonetheless able to prevent oxidation: Large carbon hydride molecules (e.g., backstreaming from the forepumps) can be physisorbed at the surface and cracked up, and these carbon atoms can react with the oxygen radicals to produce carbon monoxide, thereby keeping the surface clean. Differently from water, carbon hydrides are physisorbed to surfaces. The strength of this weaker bond increases with growing molecular mass. The ratio of absorption and desorption under ion irradiation has similar dependencies. Evidence for this chemical surface reaction is the detection of a considerable CO fraction by the RGA that was below the detection threshold without beam irradiation [16], Fig. 7. These processes were thoroughly explored by the regulated infusion of decane with monitoring feedback as the main part of the second experimental campaign. The surface can only be kept clean if the fraction of water and carbon hydrides in the residual gas are in an equilibrium, which is of course also dependent on these aforementioned parameters. If the fraction of carbon hydrides is too low the surface will oxidize. If it is too high a carbon layer will build up. Both processes are essentially irreversible. Figure 5 shows some of the results of these experiments for Ta, demonstrating the high spread in the inferred screening energies depending on the surface composition, which were verified by electron dispersive X-ray (EDX) micro analysis.

To limit the layer formation the totally implanted charge was reduced [16] Sec. 4.2. For the analysis a more sophisticated expression for the yield in Eqs. (4) and (5) was used based on a model of the target with three stacked layers [16], Sec. 4.3: a top layer consisting of either metal oxide or carbon, a deuterized zone of the metal, and the bulk of the metal containing essentially no hydrogen. Each can have different thicknesses and relative deuterium contents. The results for U_e in Fig. 5 were obtained with only the additional parameter ξ_M for the thickness of the deuterated zone in the metal in energy equivalent units of the stopping [16], Sec. 5. The differences for Ta-A and Ta-E are already considerable though the thicknesses of the surface layers were small and just started forming. Figure 4 shows the beginning of the formation of a carbon layer starting from islands that will eventually cover the whole surface, in concordance with experiences from

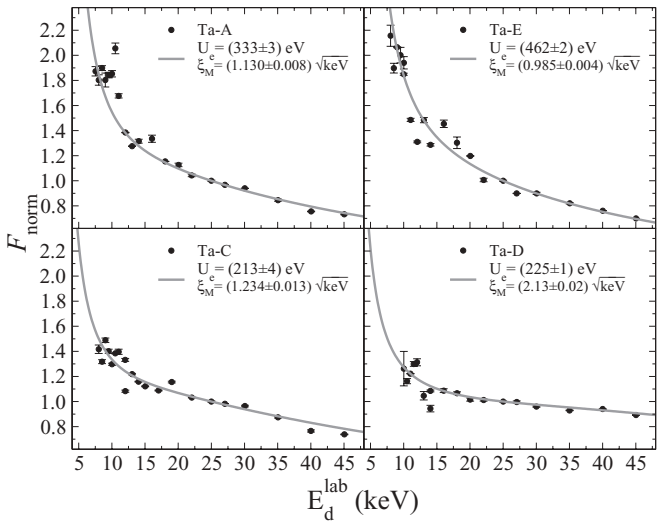

FIG. 5. Effects of different surface compositions on the inferred screening energy for Ta. Ta-A has a small C excess, Ta-E has slight C traces, Ta-C has a thick C layer, and Ta-D has a thick MO_x layer.

[3] See, for example, Ref. [35] or any surface-physics textbook.

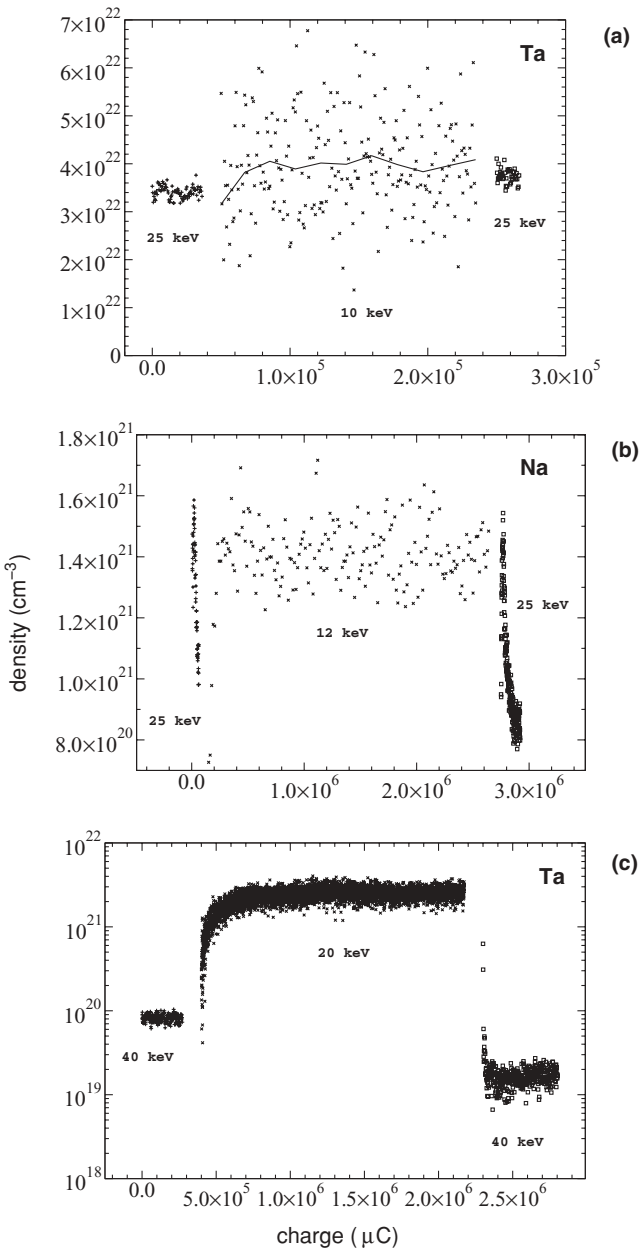

FIG. 6. Development of deuteron densities depicting counter examples to the screening enhancement as in Fig. 2. (a) A medium thick layer obliterates the screening enhancement discontinuities at high densities, here at the example of an oxide layer on Ta. The full line shows the progression from a refinement of the statistics by recalculation with an increased step size. For targets featuring low hydrogen binding ability (hence allowing only for low and unstable densities with quick profile shifts), shown are (b) a density plot of a thick metal oxide layer overtopping the ion range on a metallic Na disk and (c) an example of how heating vanquishes the hydrogen metal bond for a beam heating a 7-μm Ta foil.

thin film technology [34]. Ta-C already has a relatively thick carbon layer, which strongly reduced the screening energy, just as the metal oxide layer does in Ta-D. Those layers were just thick enough to be included in the model and allow their thicknesses to be inferred. The thickness of the

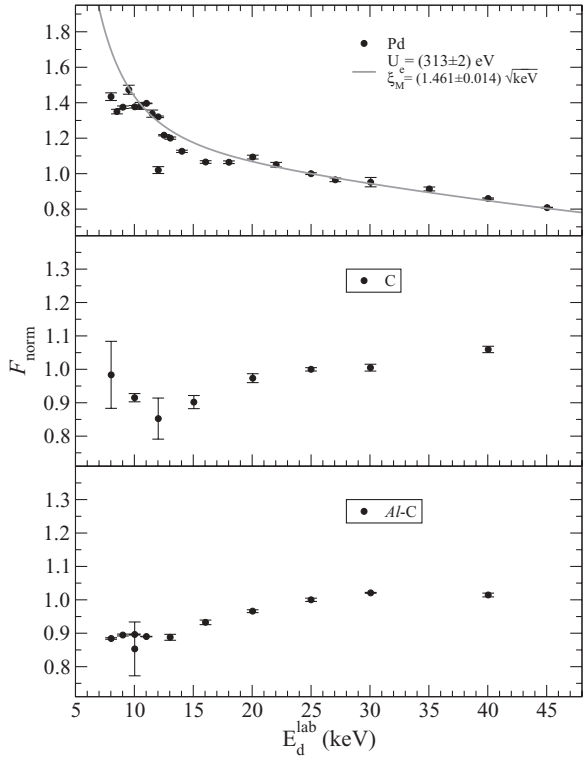

FIG. 7. Measured values of F_{norm} for Pd and carbon in two different compositions

metal oxide layer is 0.09 $\sqrt{\text{keV}}$, which conforms to about 7 nm. The corresponding screening energy would be 433 eV ([16] Sec. 5, Table 2). A thickness of 15 nm is enough to completely suppress the screening enhancement [16], Sec. 4.3. The deduced deuteron density is hardly affected and still in the vicinity of the stoichiometric ratio, as the example in Fig. 6(a) shows [Sec. 6, Figs. 13(e) and 13(f)].

Much thinner surface layers already reduce the inferred screening energy considerably. So the real value for the screening energy of Ta is possibly around 400 eV ([16] Sec. 5, Table 2). Anyhow, the screening energy values ranging from 210 to 460 eV give an sense of the systematic error originating from the surface layer formation. Carbon can achieve high deuteron densities but it does not show the electron screening effect as Fig. 7 proves. Thin deuterated carbon layers can, however, simulate a screening enhancement as inhomogeneous density profiles can do ([16] Sec. 4.3). Though the former could be excluded in our experiments, it remains a theoretical possibility when thin deuterated carbon layers form on targets containing few segregated deuterium atoms.

As already mentioned, the metal oxide contains only few segregated deuterium atoms. Those low densities are unstable and change under different conditions. For the example of a Na target with a very thick metal oxide layer the development of the calculated deuteron density is illustrated in Fig. 6(b) (see also Ref. [[16], Figs. 13(b)–13(d)]). The density estimates are calculated from the reduced yield as previously described. Before the monitor measurement at 25 keV a measurement at a low energy had been taken. Then the density quickly decreased at 25 keV. Thereafter measurements at 12 keV were started.

Now, the density very quickly increased, reaching a higher level than at 25 keV. But the discontinuity at the beginning was in the opposite direction. The density for the sequencing monitor measurement started once again at a high density and quickly decreased. The discontinuity at the beginning was once again in the wrong direction. So there is definitely no screening, in contrast to the positive case of Fig. 2. The quick shifts in the densities after the change of the implantation energy going to a "saturation" level originate from a shift of the deuteron distribution depth profile in the metal oxide linked to the different ranges of the ions ([16] Sec. 6, Fig. 14). With our method of recording a yield function $Y(q)$ over the implanted charge we can recognize those shifts and reject them. If, however, only the total yields of the long-time measurements are regarded as in the usually applied standard method (as in the other experiments discussed in Sec. V A) their comparison would erroneously lead to a screening interpretation.

The same problem arises when working with low implantation densities below the stoichiometric ratio even when the metal oxide layer is negligible. Except for insufficient implantation the density remains low if the thermal energy of the deuterons is higher than their chemical binding energy to the metal so that they can float. This applies mainly to transition metals with low ability to bind hydrogen (groups 6A–8A and 1B) or if the metals are heated. An example for the consequences of heating is shown in Fig. 6(c) for a Ta foil of 7 μm that was heated by the beam power. One observes the same behavior and no real screening enhancement. The density returns to an equal saturation level if the surrounding conditions are the same (i.e., the same beam energy, current, target heat flow, etc.). Tests with a Au foil showed a similar behavior. The most effective heat transportation mechanism in solids involves the free electron gas. Cooling the target holder has little effect since the thermal resistance at the connection is very high. Besides from heating the density profile of the deuterons in target materials with low binding ability for deuterons (metal oxides, metals with low affinity to hydrogen, and metals at high temperatures) is also changed by direct projectile hits and close phonon generation at the target deuterons depending on the beam energy. Furthermore, the metal oxide as a thermal insulator will be considerably heated by the beam power. It is therefore preferable to use thick target disks at moderate temperatures with high densities. On the other side, cooling a target to very deep temperatures would transform it into a cryogenic trap, accumulating water in thick layers on its surface prior to irradiation promoting the oxidation. The detailed investigation is covered in Ref. [6].

In summary, our data analysis method is independent of the absolute deuteron density and allows for the discrimination between changes in the reaction yield owing to the density dynamics as in Figs. 6(b) and 6(c), which are rejected, and actual changes in the cross section, which become manifest in the discontinuities at the edges of the measurements as in Fig. 2. That the discontinuities signify cross-section modifications is further ensured by analyzing measurements taken in proximity of the stoichiometric ratio only, where changes of parameters such as beam flux and temperature have, at most, marginal influence on the overall deuteron density. The error of F_{norm} is a convolution of the error from the counting statistics and long-term changes of the density. The use of high vacuum systems will inevitably cause the buildup of contamination layers. Our analysis demonstrates that those layers can only diminish the inferred screening energy since feigned enhancements from density dynamics get rejected [16], Sec. 6. The utilization of carbon hydrides embanks the layer formation, making the results in HV possible in the first place [16, Sec. 4.2]. Though the equilibrium in the residual gas between carbon hydride and water vapor is delicate and liable. So layers are present, which were examined by EDX, allowing for a relative measurement of element abundances [6]. But the thickness can hardly be quantified because of the fractal structure of the target surfaces (e.g., Fig. 4), though the model suggests that a thickness of 15 nm is sufficient to completely dispose of the screening enhancement. All in all, the obtained screening energies represent lower limits to the real value. The magnitude of the dominating systematic error from the unknown layer thickness can be assessed by the measurements in Fig. 5.

IV. RESULTS

A. Experiment

The experimentally determined results for the screening energies are summarized in Table I. The values from campaign I are in the upper part of the table. In the lower part of the table are accessory results from campaign II. In the second column of the table are the ratios of the deuterium number density to that of the host metals. Since the deuteron density can and does vary during a measurement these values are estimated averages. The values for strontium and lithium are heavily impaired by the layer formation owing to the high reactivity of both metals (especially for Li). This layer formation is expressed in the strong variations in the deuteron densities and accordingly in the reduced yields during the course of the measurement, leading to ambiguous values for the discontinuities of the reduced yields. So these screening energies should be regarded as estimations. The results were

TABLE I. Screening energies.

Metal	MD_x[a]	U_e (eV)
Ta	0.9	322 ± 15
Zr	2.1	297 ± 8
Al	0.8	190 ± 15
Sr	1.0	350–800
Li	0.03	$\lesssim 150$
Na	0.03	–[c]
Pd	0.3[b]	313 ± 2
C	–[d]	0

[a]Approximate average deuterium contents in relation to the number density of the metal.
[b]The initial implantation was deliberately prematurely aborted.
[c]An oxidation layer impeded the determination of U_e.
[d]Carbon density unknown. See text.

obtained utilizing the equilibrium in the residual gas to keep the target surface clean, which was subsequently verified by EDX analysis (see Sec. III and a more detailed discussion in Ref. [16] Sec. 4.2).

The first plot in Fig. 7 is a measurement on palladium with roughly equal residual gas conditions as for the Ta measurements [16], Sec. 5. The totally implanted charge was limited for the same reason (i.e., layer formation) as in the Ta measurements of Fig. 5.

The beam spot contains traces of carbon, specifically some dark stains [16], Fig. 8. The other two plots are the experimental proof that carbon has no screening enhancement. The drop to the lower energies originated from a lower deuterium content in the upper layers of the targets. This drop can also be caused by the voltage drop in the plasma inside the RF ion source (see Refs. [36] and [16] Sec. II), which has a higher impact for lower energies relative to the monitor measurement at 25 keV. The two carbon targets were prepared with different methods. The first one was made by deposition of soot from a ethine (C_2H_2) flame on a backing plate. A flame of ethine burning with an insufficient oxygen supply produces very pure carbon. However, the material is amorphous and rather fluffy. Accordingly, the deuteron density reaches only values of about 1.5×10^{22} cm^{-3}. The second target is a carbon film produced by the irradiation of aluminium with high decane pressure. In such a way the deposited carbon was compacted by the impacting beam ions while being forced to adopt the lattice structure of the substrate to a certain extent [37]. Hence the density of the carbon atoms is higher, and so is the deuteron density (about 5×10^{22} cm^{-3}). However, these are only estimates since the carbon densities are not known and as a result nor is the correct stopping power coefficient required [Eq. (4)][16, Eq. (10)]. In any case, the resulting enhancement factors show no significant disagreement. Thus, carbon films present no signs of electron screening. These results are listed in the lower part of Table I.

The highly reactive metal natrium corroded so easily that only low deuteron densities could be achieved and no screening was visible. Two tests with Y and Er led to thick metal oxide layers, too. In contrast from the other metals the concomitant analysis of the ^{3}He spectral peak revealed in both experimental campaigns for Li, Na, and Sr a significant suppression of the neutron reaction channel and a simultaneous alteration of the angular anisotropy [6,38].

B. Theory

From the theoretical point of view the deuterized metals can be treated as a strongly coupled plasma [8]. Since the velocity of reacting nuclei is smaller than the Fermi velocity, the electron screening effect corresponds to a static polarization of surrounding conduction and bound electrons. Consequently, the electrostatic potential energy between reacting nuclei of charges Z_1 and Z_2 shielded in a metallic medium can be described within the self-consistent dielectric function theory [18] as

$$V(r) = \frac{Z_1 Z_2 e^2}{r}\Phi(r) = \frac{Z_1 Z_2 e^2}{(2\pi)^3}\int \frac{4\pi e\varphi_1(q)\, e\varphi_2(q)}{\varepsilon_v(q)\,\varepsilon_c(q)\,q^2}\exp(iqr)\,d^3q \xrightarrow{r\to 0} \frac{Z_1 Z_2 e^2}{r} - U_{\mathrm{pol}}. \quad (8)$$

The wave-number-dependent dielectric functions ε_v and ε_c describe polarization of valence and core electrons, respectively, of host atoms induced by a charged impurity and take into account the short-range electron correlation and the exchange interaction between electrons (for details see Ref. [18]). The functions $\Phi(r)$ and $\varphi_i(q)$ are the screening function and electronic charge form factors of reacting nuclei, respectively. At small distances (applicable for nuclear reactions and decays) the potential energy can be approximated by using the energy-independent polarization screening energy U_p, which scales with the product of the charges of the involved nuclei. For the d+d reactions we used the self-consistent charge form factor $\varphi(q)$ within the Thomas-Fermi approximation [18,39]:

$$\varphi(q) = 1 - z + \frac{zq^2}{\left(q^2 + k_{\mathrm{TF}}^2\right)}. \quad (9)$$

Here, the Thomas-Fermi wave number $k_{\mathrm{TF}}^2 = 6\pi e^2 n/E_F$ has been applied; n and E_F are the electron number density and the Fermi energy, respectively. The number z corresponds to the fraction of electrons bound to deuterons and is for metals close to unity. Since we are interested in the evaluation of the strongest possible screening effect, we uniformly set $z = 1$ for all target materials. In the absence of screening, $\varepsilon_v \equiv \varepsilon_c \equiv 1$, $z = 0$ and $V(r)$ reduces to the bare Coulomb potential [$\Phi(r) \equiv 1$].

In the metallic lattice, besides electrons also positive ions can contribute to the screening of the Coulomb barrier between reacting nuclei. This effect, called cohesion screening [18], can be calculated as a gain of the potential energy of two deuterons in the lattice field of the host metal compared to that of the helium atom produced in the fusion reaction. To calculate the potential energies we used the universal ion-ion interaction given by Ziegler, Biersack, and Littmark [40]. For a rough estimation of the cohesion screening energy U_{coh}, we calculated the potential energy gain resulting from the surrounding 12 host atoms assuming the same fcc crystal structure for all target materials investigated. The cohesion screening is a slowly increasing function of the atomic number. The total screening energy is the sum of both contributions: $U_e = U_{\mathrm{pol}} + U_{\mathrm{coh}}$.

The results of the theoretical calculations obtained for the d+d reactions taking place in different metallic targets are presented in Fig. 8 together with our experimental values. The electron screening energies moderately increase with the atomic number of host atoms [15], reaching for heavier nuclei the value of about 300 eV. The experimental target material dependence agrees with the theoretical expectations. However, the experimental screening energies are larger by a factor of about 2 compared to the theoretical values. Since the experimental screening energies obtained for insulating materials are much smaller (<50 eV) [15], and taking into account that the screening contributions arising from polarization of bound host electrons and cohesion should be similar for both metallic

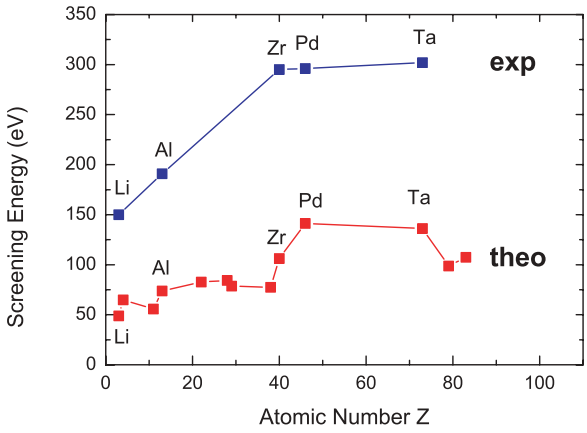

FIG. 8. (Color online) Comparison between experimental and theoretical screening energies.

and insulating targets, we can conclude that the enhanced screening effect results from conducting electrons. Thus, for a comparison among different target materials the electron-gas parameter $r_S = [3/(4\pi n)]^{\frac{1}{3}}/a_0$, where n and a_0 are the valence electron density and the Bohr radius, respectively, is much more suitable. Using this parameter, we display the experimental polarization screening energies obtained by subtraction of the theoretical cohesion contribution in Fig. 9 together with the theoretical polarization screening energies.

Now, the quality of the theoretical description is much more visible. In contrast to the simple Thomas-Fermi model [39], providing for free electrons a smooth dependence of the screening energy given by $U_{\mathrm{TF}} = Z_1 Z_2 e^2 [4/(\pi a_0)]^{\frac{1}{2}} (3\pi^2 n)^{\frac{1}{6}} = 2 Z_1 Z_2 e^2 [9/(4\pi^2)]^{\frac{1}{6}} r_S^{-\frac{1}{6}}$, the dielectric function theory describes fluctuations of the experimental polarization screening energy very well. The fluctuations result from the polarization of bound (core) electrons, whose contribution to the total screening energy depends very strongly on their binding energy [18]. If the bound electron contribution is eliminated from the experimental polarization screening energies we get

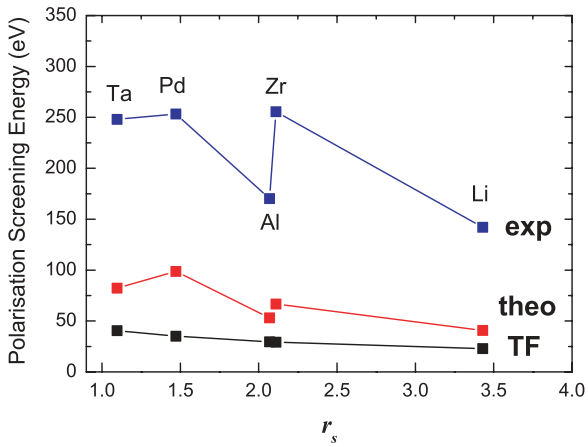

FIG. 9. (Color online) Experimental and theoretical polarization screening energies vs the electron gas parameter r_S. For comparison the Thomas-Fermi screening of the electron gas is presented.

experimental values for the free electron polarization that can be parametrized by a smooth dependence on r_S : $U_{\mathrm{pol},f} = Z_1 Z_2 (250 \pm 20)\,\mathrm{eV}/r_S^{\frac{1}{2}}$. This result can be used for an estimation of the free electron contribution in the metallic environment to the screening energy in reactions between nuclei with charges Z_1 and Z_2. In contrast to the d+d reactions, the contribution coming from electrons bound by heavier reacting nuclei is much larger and should be included separately. This can be calculated as the gain in electron binding energies between distant atoms and the final united atom. Similar results can be obtained by using the Thomas-Fermi model, leading to $U_{e,b}(TF) = 1.13 Z_1 Z_2 e^2 (Z_1^{\frac{1}{2}} + Z_2^{\frac{1}{2}})^{\frac{2}{3}}/a_0$ [41]. In the case of heavier nuclei the cohesion screening energy can be neglected, since the strength of the interaction with the lattice atoms increases much more slowly than the product $Z_1 Z_2$. Thus, the total screening energy is only the sum of the free electron and bound electron contributions. The same estimation can also be applied for radioactive α and β decays [41].

Dielectric function theory does not predict any temperature dependence of the polarization screening energy unless the electron density of the target material remains constant and the projectile velocity is smaller than the Fermi velocity, which is typical for a strongly coupled plasma. For velocities higher than the Fermi velocity the electrons are unable to follow the ions and the electron screening gets weaker. In this limit of a weakly coupled plasma (Debye-Hückel limit) the screening length becomes larger than the mean atomic distance and the classic description of electron screening is applicable. The screening energy is inversely proportional to the square root of the kinetic energy or equivalently of the plasma temperature ($U_e \sim \frac{1}{\sqrt{E}} \sim \frac{1}{\sqrt{T}}$). An analytical formula connecting both limits has been derived by Lifschitz and Arista [42] for the stopping power of moving ions in the electron gas and can be applied for the electron screening in nuclear reactions [15]. Thus, the velocity dependence of the screening energy can be given as follows:

$$U_{\mathrm{dyn}}^2 = U_{\mathrm{ad}}^2 \left[\frac{1}{2} + \frac{v_F^2 - v^2}{4 v_F v} \ln \left| \frac{v + v_F}{v - v_F} \right| \right], \qquad (10)$$

where U_{dyn} and U_{ad} denote dynamic and adiabatic screening energies, respectively. The Fermi velocity v_F depends on the electron density and therefore is characteristic for the target material. This relation calculated for the d+d reactions in the Ta environment is presented in Fig. 10.

The energy dependence of the Debye-Hückel screening is also shown in Fig. 10. It is seen that the electron screening can be described by the Debye-Hückel theory only for projectile energies higher than the Fermi energy (the Fermi energy of deuterons in Ta amounting to about 56 keV) or equivalently for temperatures higher than the Fermi temperature ($\sim 1.8 \times 10^5$ K for Ta). Thus, in the cases discussed here, the Debye-Hückel screening is not applicable for both nuclear reactions and radioactive decays.

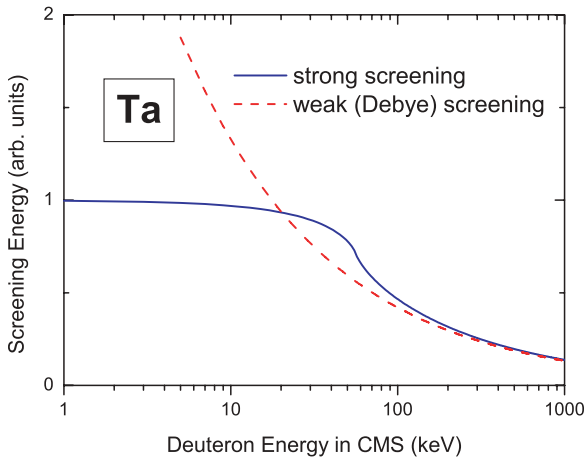

FIG. 10. (Color online) Screening energy dependence on the projectile energy. The Debye screening is applicable only for deuteron energies larger than the Fermi energy (56 keV for Ta) or equivalently for plasma temperature larger than the Fermi temperature (1.8×10^5 K for Ta).

V. COMPARISON WITH OTHER EXPERIMENTS

In view of the augmented information provided by our differential analysis method and experimental procedure the results of other groups will be discussed.

A. *d*+*d* Experiments

In Fig. 11 an overview of screening energy results and appendant deuteron densities from other experiments is plotted. All were carried out in high vacuum systems and hence suffer from the same progressive oxidation process under ion irradiation with the inherent problems noted in Sec. III and Ref. [16]. A quick glance already shows that the screening energy results are pretty much scattered and do not reveal a pattern. But in conjunction with the deuterium metal ratio (the deuteron density) peculiarities become evident. Our high screening energy results (Table I) were achieved at high absolute densities in the proximity of the chemical stoichiometric ratio where the ion beam flux has no influence on the target deuteron distribution, whereas the high screening results of the other groups were exclusively attained at low deuteron densities (10^{-1}–10^{-2} below the metal number density). Complementary high densities did not yield enhanced screening in those experiments. Both classes of screening results are associated with groups in the periodic table, exposing the chemical relationship with respect to the surface reactions and hydrogen binding ability of the targets as described in Sec. III. This is particularly manifested in Fig. 11 for the group 3A metals, including the lanthanides, which have low screening values at high densities and conform to the counter example case of Fig. 6(a). But also the transition metals show three clusters of high screening results at low densities in Fig. 11, corresponding to the cases of Fig. 6(b) and Fig. 6(c), respectively. These correlations will be substantiated in the following.

1. The Garching experiment

The first accelerator experiment aimed are searching for modifications of the cross section in the *d*+*d* fusion reactions caused by the metallic environment was done on Ti [43]. No enhancement could be observed. The measurements were performed on a 3-μm-thick Ti foil fixed in a copper target holder frame with flow channels for liquid N_2 cooling and a thermocouple for temperature determination. No effort was made to specify the deuteron density in the target. Instead a fixed value from material research was adopted, which is inadequate because the deep cooling of the target water that accumulates on its surface produces under ion irradiation a

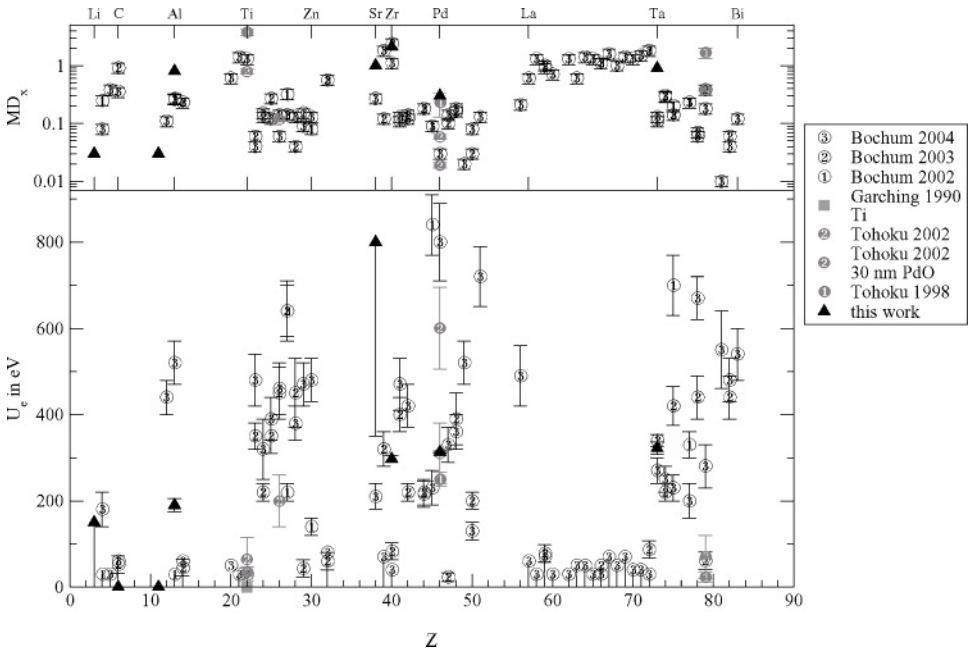

FIG. 11. Overview of screening experiment results. Top: Deuterium to metal ratio x. The values for x of Ref. [10] were estimated from Fig. 2 therein. The values of Ref. [14] are the data base; data points from Refs. [12,13] are included only if they differ. Bottom: Screening energies U_e. Legend: Garching 1990 [43]; Tohoku 1998 [9], 2002 [10]; Bochum 2002 [12], 2003 [13], 2004 [14].

considerable oxide layer.[4] In addition, the beam current up to 0.1 mA leads to a distinct temperature increase inside the deacceleration volume of the ions in the thin foil, which will also alter the density profile away from the supposed unit value. All further measurements on Ti in Fig. 11 resulted in very low screening values with densities in proximity of the chemical stoichiometric ratio. The higher the deuteron density, the lower the screening value. Ti is chemically very similar to Zr, as both belong to group 4A. From our experience Zr oxidizes readily. So a relatively thick metal oxide layer, corresponding to the third case in Ref. [[16], Figs. (13e) and (13e)] [Fig. 6(a)] explains the results.

2. *The Tohoku experiments*

The results of Refs. [9,10] are based on the analysis of the total yield of the proton measurements [9, Eq. (1)] with one detector at a laboratory angle of 90° and at a projectile energy $E_{\mathrm{d}} \in [2.5, 10]$ keV,

$$Y_t(E_d) = \varepsilon N_D \int_0^{E_{\mathrm{d}}} \sigma(E) \left(\frac{dE}{dx}\right)^{-1} dE, \tag{11}$$

after depth energy substitution (Sec. II), with a proton detection efficiency ε, a cross section parametrizationσ of Ref. [44], and finally the target deuteron number density N_D, which is presumed to be constant for all energies and ranges. With the stopping power relation the additional error of the stopping power coefficients is introduced. To determine and observe the density value, repeated monitor measurements were performed at 10 keV. The density was then calculated from the yield Y_t(10 keV) by solving Eq. (11) for N_D with the supposition that the screening enhancement is negligible there. According to the not unambigious text (see Ref. [10] and suitable back references) for the quantification of the enhancement and extraction of the screening energy the yields are normalized to the experimental one at 10 keV, thus becoming independent of the actual value of N_D:

$$Y_{\mathrm{norm}}(E) = \frac{f(E) \cdot Y_t(E)}{Y_t(10\ \mathrm{keV})}, \tag{12}$$

$$f(E) = \frac{Y(E)}{Y_{\mathrm{bare}}(E)} = \exp\left(\pi\eta(E_{\mathrm{c.m.}}) \frac{U_e}{E_{\mathrm{c.m.}}}\right), \tag{13}$$

where the theoretical expression for the thick target enhancement factor f is simply adopted from the approximated term in Eq. (7) of Ref. [2] for the enhancement of the cross sections in thin targets. This expression is, however, derived for cross sections based on an increase of the effective projectile energy. It might be introduced in the integrant in Eq. (11) and must not be pulled out of the integral in that manner. A thick target enhancement factor should retain the energy integration as in Eq. (6). The approximation in Eq. (7) is only valid for $E_{\mathrm{c.m.}} \gg U_e$, which is no longer fulfilled by the given experimental circumstances with beam energies of some keV and screening energies of several hundred eV. This also means that the supposition of a negligible screening enhancement at 10 keV is no longer valid either. Moreover, Eq. (13) diverges for energies approaching zero. Although the invalid approximation leads to an underestimation of the derived screening energy, the neglect of the enhancement at 10 keV effectuates a gross exaggeration because the curvature of the enhancement curve must be greater to describe the steeper slope of the data (in analogy to the difference in curves 1 and 2 in Ref. [16], Fig. 12. The inclusion of measurements taken at higher energies would have revealed this. The deuteron density value obtained at 10 keV ought be heavily altered, too. The target holder was cooled with liquid N_2. The constancy (and subsequently deduced the homogeneity) of the density in the target was investigated by measurements at 10 keV with target heating from different beam fluxes or a mounted heater in the case of Pd in the interval $[170, 230]$ K determined with a thermocouple. The results in Ref. [10], Fig. 1 show a strong dependency of the "saturation" density on the target temperature and material with a considerable general decrease with rising temperatures. The density descends from Ti over Au, Fe, and Pd to PdO. Conspicuous are the differences in the deuteron densities between Refs. [9] and [10] for Ti, Au, and Pd, which are almost one order of magnitude, whereas the corresponding screening values accord within their errors (Fig. 11) though the latter U_e are generally higher. This discrepancy remains unexplained in Ref. [10]. Although Au and Fe do not build up firm bonds to hydrogen the achieved densities are proportionally higher at these deep temperatures. A deliberately produced 30-nm-thick PdO layer on a Pd target in Ref. [10] yielded an especially high screening energy with an especially low density. Such a thick PdO layer would show quick shifts in the deuteron density profiles with higher averaged densities at lower projectile energies, such as in the second case in Ref. [[16], Fig. 13(b)–13(d)][Fig. 6(b)] when changing the projectile energy and using the differential analysis method. So this large screening is simulated by the density alteration during the total yield measurement. The density in the Pd target of Ref. [10] is noticeably low, which points to the formation of an oxide layer distinctly thicker than on the Ti target, approaching that of the PdO target. This means that the screening value is also generated by density dynamics and the agreement with our value is by chance. Even though our Pd value was obtained from measurements with a limited total ion dose and still growing densities prior to saturation to minimize surface contaminations, the highest density of all experiments was achieved. Although the targets as described in Ref. [10] are thick enough (∼1 mm) to guarantee an effective heat transport in the bulk of the material by the electron gas, the heterogeneous target Au/Pd/PdO with a total thickness

[4]This interpretation is confirmed in Ref. [[43], Fig. 3]. There the proton counting number is plotted over the implanted charge with a coarse resolution. The gradient of this curve is proportional to the yield and the deuteron density [Eqs. (1) and (2)]. The curve should be linear at and after saturation. At 0.2 C there is a hump in the curve, after which the gradient is clearly lower than before. The authors explain this by a hydrogen release from the foil because of a small temperature increase. However, the gradient remains significantly below the previous value, which altogether rather complies to the curve from a metal oxide buildup reported in Ref. [16], Fig. 6, C/O = 0.4.

of only 60 μm (with 0.1 μm Au) [9] is too thin, therefore leading to a considerable temperature increase in the beam stopping volume, which is to this extent not detectable by any outside mounted thermocouple. So, the observed high screening energy of (602 ± 23) eV can be explained by the shifts in the density profile from elevated temperatures as in Fig. 6(c) [[16], Fig. 13(a)] and the heterogeneity of the target and accordingly the density.

To explain the ascertained relation between the screening energy and the density depicted in Ref. ([10], Fig. 4) (i.e., the high screening associated with low deuteron densities), the concept of a deuteron "fluidity" was introduced in Ref. [10] whereby fluid deuterons and conduction electrons are to behave like a hot plasma. But in palladium oxide there are no conduction electrons. In view of the stated density dynamics this explanation breaks down. The explanation by density dynamics is also sustained by the significantly larger standard deviations of the repeated density measurements at 10 keV for targets with low densities in Ref. [10], Fig. 2. Indeed, the saturation density in our experiments returns to the same level for the same conditions but with higher deviations. To avoid the observed temperature changes of the deuteron densities in the targets the beam current was adapted in such a way to maintain a constant power input into the target. Although in Ref. [10] is admitted that this procedure does not keep the power density constant by reason of the stopping power relation, the mobility of the deuterons is influenced not only by the indirect ambient temperature but also by direct ion interaction and changes in the distribution of the stopped projectile deuterons. The authors conceded that they were unable do detect possible short time changes in the proton counting rate. With our differential method we did not observe any discontinuity belonging to screening on oxidized targets, with low absolute densities being independent of the actual beam current and power input. The most trustworthy screening value seems to be the result for Au in Ref. [9] obtained at a high density, which conforms our test with a Au foil at a very low density yielding no enhanced screening. But under ion irradiation even noble metals can oxidize.

Very recently experiments have been continued using the same accelerator setup, procedure, and analyzing method as described here [45]; consequently, the same considerations apply. As before the target holder was cooled with liquid N_2, further approaching the boiling temperature of nitrogen. For the Sm target a screening energy of (520 ± 56) eV was deduced.[5] But, unlike in the previous publications, not even an estimate for the deuteron density was given. The high statistical errors in Ref. [45], Fig. 5 and the vague statements regarding the deuteron "fluidity" obtrude the inference of a low density with the same consequences, too.

3. *The Bochum experiments*

The largest data set of screening energies is provided by Refs. [12–14]. The applied experimental procedure and data analysis method explained in Refs. [11,12] is exactly the standard strategy in nuclear astrophysics as described in Ref. [46] including measurements of relative excitation functions with normalization to known cross sections. As such it is a step back behind Ref. [9], where already concessions to the special situation of hydrogen in metals were made. Again just the total yield for the thick target of the measurement of the protons with four detectors at a polar laboratory angle of $\theta = 130^\circ$ at an energy $E_d \in [5, 30]$ keV was determined. The total yield $Y(E_d, \theta)$ was repeatedly taken at fixed energies with equal step sizes Δ of 0.5 and 1.0 keV for $E_d > 10$ keV, from which an energy differentiated yield $Y'(E_d, \theta)$ is calculated [Eq. (14)] to extract the cross section [Eq. (15)] [11, Eqs. (5), (7), and (8)][6]:

$$Y'(E_d, \theta) = [Y(E_d, \theta) - Y(E_d - \Delta, \theta)]/\Delta \quad (14)$$

$$= \sigma(E_{\text{eff}})\varepsilon_{\text{eff}}(E_d)^{-1} \times \underbrace{\Omega K_\Omega(E_d, \theta) W(E_d, \theta).}_{\alpha \stackrel{!}{=} \text{const.}} \quad (15)$$

The energy integration prior to Eq. [15] vanished by means of the mean value theorem of calculus, leaving behind the integrand to be evaluated at the effective energy $E_{\text{eff}} \in (E_d - \Delta E_d)$, where one-half of the yield is attained. Except for σ for all other factors in Eq. [8] it is assumed that their change within the energy interval can be neglected. Moreover, the angular terms are collected in the factor α, which is supposed to be constant for the whole energy range of the measurement. In Eq. (15) Ω is the solid angle of the detectors, K_Ω is its transformation to the c.m. system, and W is the angular distribution of the reaction yield. Differently, therein the stopping cross section ε [i.e., the energy loss per particle areal density in eV/(atoms/cm^2)] is used, and not the linear stopping power $\frac{dE}{dx}$ (in keV/μm). The effective stopping cross section is assembled from the one for deuterium and the host metal [11, Eq. (9)]:

$$\varepsilon_{\text{eff}}(E_{\text{d}}) = \varepsilon_D(E_d) + x\varepsilon_M(E_d), \quad (16)$$

with the metal atom fraction $M_x D$. Thus, the dependence of the composition of the target is completely shuffled from the stopping factor into x. Consequently, the deuteron density described by x is forced to be fixed for all projectile energies, the range in the target, and the whole measurement series on the target. For the determination of the absolute value of the cross section in Eq. [8] x was scaled to a known cross section for gaseous deuterium [7] at $E_d = 30$ keV. This means that the deduced uniform deuteron density for the whole measurement series is only dependent on the one value at 30 keV and only there validated, at most. So this method is even less sensitive to changes of the density during the course of the experiment than in Ref. [9]. Then the S factor is calculated. The screening energy is obtained from another fit to the S-factor data with three parameters of the expression in the second line of Eq. (7) together with a linear S-factor function. Furthermore, additional error sources were introduced without need by

[5]The experiment was meant to sustain the temperature dependence of the inapplicable Debye model [Eq. (19)].

[6]The symbol names used by the authors have been changed for the sake of the uniformity of notation and comparability.

sticking to the standard procedure: repeated yield differences at fixed energies, introduction of the effective energy, the stopping power coefficients, and S-factor computation. The errors of the computed S factors are said to be dominated by the spread in the yields Y' from various runs (see Refs. ([11] Sec. 4, p. 380) and ([12] Sec. II, p. 195)); that is, the yields were repeatedly measured with stepwise increasing and decreasing beam energies. (This implies that the errors from different Y values are distinctly higher than the corresponding statistical errors, which can be seen in Refs. [12,14], Fig. 1). As can be seen from the position and error bars of the data points in Refs. [12,14], Fig. 1 the differences of the Y values must be significant. This is consistent with our experience that the density profile returns to the same depth-averaged value for the same surrounding conditions but with higher deviations at lower densities. The comparatively large errors relative to the number of the data points from the nonlinear fit routine for the parameter U_e reflect a significant correlation between the three fit parameters (as could have been read off the covariance matrix) and hence will help to judge the capableness of the applied model.

From Fig. 11 one can recognize once again the conspicuous connection between the deuteron density and the screening energy as in the data of Refs. [9,10]. High densities are linked to low screening energies because of moderately thick metal oxide layers as in the third case of Ref. [[16], Figs. 13(e) and 13(f)] [Fig. 6(a)]. Examples are the elements of the groups 3A ($_{21}$Sc, $_{39}$Y, and the lanthanides $Z = 57$–71) and 4A (Ti, Zr, and $_{72}$Hf), emphasizing the chemical kinship with regard to the described surface reactions in Ref. [16], Sec. 4.1 (Sec. III). Low densities generate high screening energy findings owing to shifts in the density profile either in thick metal oxide layers or materials with low hydrogen binding ability as in Ref. [[16], Figs. 13(a)–(d)] [Figs. 6(b) and 6(c)]. This relationship can be recognized at the transition metals (groups 6A–8A: $Z = 24$–28, 42–46, and 74–78) for example. It is argued in Ref. [12] that the large enhancement findings are most likely due to electron screening because the data could be fitted well with the screening parameter U_e. In view of the dispersion of the data points in Refs. [12,14], Fig. 1 their functional progression can also be described with the target model of Ref. ([16] Sec. 4.3), which implements a simple static step function for the density profile. The model can mimic an exponential-like increase toward low energies quite passable by an inhomogeneous density profile with a superdeuterated surface layer alone without screening enhancement (i.e., $U_e \equiv 0$) [[16], Fig. 10(c)]. A existing screening increase can also be largely exaggerated by the density profile of a deuterated zone in the metal with a limited thickness [[16], Fig. 10(d)]. Those were only static density profiles. A density profile dynamically changing with the energy as vindicated by Fig. 6 [16], Fig. 13 could perfectly imitate the exponential-like screening enhancement given the data distribution. In contradistinction thereto our data do not allow for such a description as quantitatively demonstrated in Ref. [16] Sec. 5, Fig, 12. The Monte Carlo code SRIM for the simulation of ion stopping processes in matter was used to ratify the assumption of a homogeneous depth distribution of the deuterons over the range of the ions [11]. But SRIM does not take into account the ability of hydrogen to diffuse. The homogeneity assumption was experimentally reconfirmed by a subsequent off-line ERDA on a 4-MV tandem accelerator with the outcome that the distribution is uniform within 10% for most materials [12]. Self-evidently a subsequent examination cannot detect dynamic changes but only the state of thermodynamic equilibration. With the problem of oxidation have been pointed to [47], RBS analysis was performed on the targets with the result that there were "no detectable surface contaminations" with the exception of Al where there was an Al_2O_3 layer with a thickness of about 150 monolayers [13,14]. Those findings prove that the resolution and sensitivity of the applied analysis techniques are too low; at least the passivation oxide layers from the unavoidable exposition to air with the used equipment should have been visible. For both ERDA and RBS it is valid that light projectile ions with a kinetic energy of some MeV cannot provide the wide enough energy spectrum of ejectiles necessary to resolve single atomic layers. Therefore a HIERDA with incident energies of heavy ions on the order of 0.1 GeV would be required with sophisticated magnetic analyzing systems (e.g., Ref. [37]). This is additionally complicated by the circumstance that these methods deliver expressive results only if heterogeneous samples are made up of well-defined layers. This is not fulfilled for the implantation targets with indistinct chemical composition and surfaces fractalized by embrittlement and beam deterioration [Fig. 4; see Ref. [16], Fig. 8]. So with the applied methods one cannot detect metal oxides with a thickness of a few tens of monolayers (some nanometers), which is already sufficient to obliterate the screening enhancement (Sec. III; see Ref. [16] Sec. 4.3) wheras they are not thick enough to affect the applied density determination at 30 keV significantly.

The thick oxide layer found on Al was defined to be of natural origin because the property of Al to readily oxidize in air. Hence a Kr ion sputtering treatment at 15 or 35 keV was applied prior to the implantation measurements to remove those natural metal oxide layers, which is the main difference among the results of Refs. [12–14]. This procedure does not take into account that the major cause of the oxidation is contributed by the water in HV systems under deuteron irradiation, which keeps going on nevertheless. Although the high sputter yield of the Kr ions may allow for a surface cleaning, the large Kr atoms thoroughly destroy the crystal structure of the target and get trapped in the material fractalizing the surface and thus possibly even promoting the oxidation process under subsequent deuteron irradiation since the necessary annealing step is omitted. The deviations in the screening energies among Refs. [12–14] are in both directions, giving an indication of the magnitude of the true error in the determination of the screening energies in this way similar to our experiments on Ta (Fig. 5). Whether the increase or decrease of the screening finding comes from an increase or decrease of the thickness of the oxide layer, or low hydrogen binding ability of the metal, or a too thin overheated target foil can scarcely be told afterward on the basis of the available information. But there are peculiarities. It becomes unclear which beam currents were used (i.e., 54, 5, or 2.4 μA) and how they influence the stability and the inferred screening

values. In Ref. [12] it was reported that instable yields depend on the beam current for In and "other elements with a low melting point."[7] The elements of group 1B (Cu, Ag, and Au) had a small screening value in Ref. [12,13], consistent with the gas target value that became large in Ref. [14]. That is in contradiction to the very low screening energy for Au of Ref. [9] and our finding of no screening. The extraordinary high screening value for Pd does not change with the Kr sputtering but matches best to the PdO value of Ref. [10], which is another proof for the nevertheless continued oxidation process. Owing to the moderately thick metal oxide layer and the stable deuteron density close to the stoichiometric ratio the metals of groups 3A and 4A, including the lanthanides, neither allow for a real screening observation nor a simulated screening by density dynamics in the experiment of Ref. [14]. In the coextensive publications [25,26] these metals where heated to 200 C thus overcoming the chemical bond between the metal atoms and deuterium conveying it into segregation and leading to a density drop of two orders of magnitude; that is, the case of Ref. [[16], Figs. 13(e) and 13(f)] [Fig. 6(a)] is transformed to that of Ref. [[16], Figs. 13(a)–(d)] [Figs. 6(b) and 6(c)]. The then observed high screening energies again can be informally explained by the density dynamics owing to the high mobility of the deuterons induced by the high temperature and conjectural promoted metal oxide layer formation. This is made clear with the example of Ti where five data points taken at different temperatures show the transition in Refs. [25,26], Fig. 3. In Ref. [13] difficulties in attaining stable reaction yields for Ta at high temperatures were reported, but these were not subsequently further elucidated. The stability test for the density in Ref. [25] is inapplicable since the analysis method used cannot recognize the short time changes of the density.

The intention of these experiments was to find a connection between the observed screening energy and some electronic properties of the elements, something that is to be underscored since it is an important step toward the understanding of this phenomenon. The authors propose the Hall coefficient to be this quantity, stating that the effective density n_{eff} of the free charge carriers (i.e., electrons and holes likewise) form a Debye sphere R_D around the deuterons and thus generate the screening potential [13]:

$$R_D = \sqrt{\frac{\varepsilon_0 kT}{e^2 n_{\text{eff}} \rho_a}}, \tag{17}$$

$$U_e = \frac{e^2}{4\pi\varepsilon_0}\frac{Z_p}{R_D} \tag{18}$$

$$= \frac{e^3 Z_p}{4\pi\varepsilon_0}\sqrt{\frac{\rho_a}{\varepsilon_0 k}}\sqrt{\frac{n_{\text{eff}}}{T}}, \tag{19}$$

with ρ_a the number density of the atoms, T the temperature of the free electron gas, and Z_p the atomic number of the projectile. The classical Debye screening is, however, not applicable for low temperatures (electron energies below the Fermi energy) and dense plasmas (solid states) where quantum mechanical effects dominate and the screening effect depends only on the charged particle density and not on the temperature [1,15,41]. Additionally, the motion of the bound electrons simulating the hole is not free but governed by quantum mechanical tunneling between neighbor atoms. The fact that the screening energy is vanishing for high deuteron densities is explained by the assertion that these metal hydrides are insulators. This is not right for the majority of the metal hydrides, which are metallically or covalently bound and retain their metallic properties. In fact, the electrons of the hydrogen are added to the conduction band of the metal. The Baranowsky curve of the electric resistance of metal hydrides shows that the resistance at the chemical stoichiometric ratio is even lower than for somewhat lower densities and comparable to the metal [33]. By using a ^{3}He beam on a deuterated $_{78}$Pt target via the reaction $d(^3\text{He}, p)^4\text{He}$ [12] a screening energy was inferred that was about twice as high [(730 ± 60) eV at 1–3 μA] as for the d beam [(440 ± 50) eV], which was regarded as a confirmation of the Z_p dependency [Eq. (19)] of the Debye hypothesis [13]. In Ref. [14] however, the screening energies for ^{3}He [(680 ± 60) eV] and d beams [(670 ± 50) eV] at Pt became equal without explanation. The inconsistency of the Pt data also comprises the measurements [25,26]) for the verification of the temperature dependence [Eq. (19)] of $T^{-\frac{1}{2}}$. With the exception of the room temperature data point the other four data points are equal within their error interval. So the temperature dependence is based on a single uncertain point. Furthermore, the findings for the metals of groups 3A and 4A are in contradiction to it, which cannot be resolved by the introduction of a high-handed function [25,26], Eq. (4).

To arrive at a more quantitative assessment of the hypotheses, methods of statistical data description and analysis can be applied (e.g., Ref. [48]). Of the 58 examined elements in Ref. [14], Table 1 the effective charge densities calculated from the Hall coefficient R_H are selectively specified for the 25 elements with high screening values only, because the authors erroneously precondemned the others to be insulators with zero charge carriers. Effective charge densities for the elements In, Sn, Sb, Pb, and Bi, which do not fit in the explanation scheme, were also omitted.[8] It needs to be

[7] In Ref. [14] In has a very high screening value (likewise the elements Bi, Tl, and Zn which have also a low melting point) without explanation whether the problem has been solved or simply ignored. The elements Rh, Re, and Ir were measured with a beam current of 2.4 μA in Ref. [12], resulting in high screening energies, which decreased considerably in Refs. [13,14]. Re decreased from (700 ± 70) eV over (420 ± 45) eV to (230 ± 30) eV, indicating a beam current dependence even though these elements have high melting points.

[8] The Hall coefficients originate from Ref. [49]. In Ref. [13] the values for n_{eff} for Sn and Pb in Table 1 were left out on the grounds that they were unreasonably high (table footnote f). In Ref. [14], Table 1 the values for In (−82), Sn (−84), Sb (−0.09), Pb (21), and Bi (-4×10^{-4}) were omitted without vindication (with the values for Sb and Bi being much smaller than expected). Instead the Hall coefficient for Pd was remeasured with a better fitting result, giving reason to doubt other values for the Hall coefficients. But no description of the measurement procedure was given.

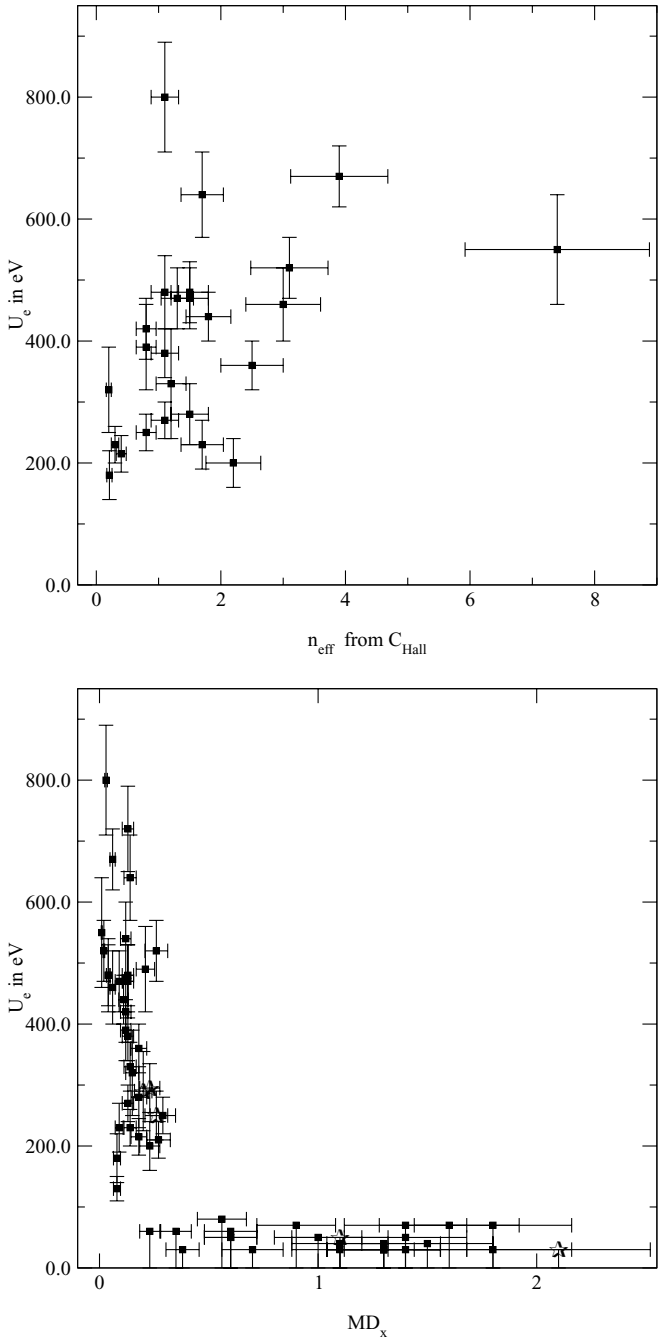

FIG. 12. Scatter plots of (top) $U_e \leftrightarrow n_{\text{eff}}$ with n_{eff} from the Hall coefficient C_{Hall} and (bottom) $U_e \leftrightarrow x$ with x being the deuterium contents in the compound MD_x. The star denotes temperature-dependent points for Ti.

particularly pointed out that the authors impose a flat error of 20% on the Hall coefficients contrary to the original experimental uncertainties. Both have severe impact on the interpretation.

A visual survey based on Fig. 12 already shows that the distribution in the scatter plot for the case of $U_e \leftrightarrow n_{\text{eff}}$ is rather dispersed whereas the distribution for $U_e \leftrightarrow x$ roughly indicates a hyperbolic connection. The temperature-dependent data points for Ti [25,26], Table 1 are additionally included in the bottom scatter plot (tagged with a star), demonstrating the transition from a high stable density to a low instable density thus allowing for density dynamics that simulate the high screening findings. Three testing methods for continuous variables were used: Pearson's linear correlation r, in which a linear association between the variables is assumed, the Spearman rank correlation r_s, which measures the monotonic association between the variables and is therefore invariant under monotonic transformations, and Kendall's τ, which is even more nonparametric since it uses only the relative ordering of the ranks by counting the inversions in the paired data points. Kendall's τ also enables the easy inclusion of errors by adaptive binning. Both r_s and τ are robust in opposition to the linear correlation. All such tests attempt to falsify the null hypothesis of no correlation. Their correlation coefficients describe the strength of the correlation, in the range $[-1, 1]$, where 0 stands for no correlation and $(-)1$ for total (anti)correlation. Complementary, the P value determines the significance of the obtained correlation: The lower P the higher is the significance. The results tend to be congruent; representatives from the Spearman rank correlation are listed in Table II.

TABLE II. Spearman rank correlation tests.

Number[a]	Correlation	r_s	P value
1	$U_e \leftrightarrow n_{\text{eff}}$	0.4894	0.0130
2	$U_e \leftrightarrow x$	−0.7997	5.1404×10^{-14}
3[b]	$U_e \leftrightarrow n_{\text{eff}}$	0.2830	0.0768
4[c]		0.1240	0.4171
5[d]		0.0174	0.9096
6[b]	$U_e \leftrightarrow x$	−0.7466	2.3602×10^{-16}

[a]Data of Ref. [14], Table 1.
[b]Including data from Refs. [25,26], Table 1.
[c]Including data from Refs. [25,26], Table 1 and n_{eff} for the omitted elements.
[d]Additional consideration was taken of the sign of the Hall coefficient.

The assumed functional dependency in Eq. (19) is tested on the restricted data set [14], Table 1 (#1); the correlation coefficient is below 0.5 with a low significance. In contradistinction thereto the correlation to the density x has considerably higher values with utmost strong significances (#2). Including the temperature-dependent data [25,26], Table 1 into the calculations leads to a considerable decrease in the correlation coefficient (#3), which is further reduced when n_{eff} for the omitted elements In, Sn, Sb, Pb, and Bi is regarded (#4), with a concurrent decrease in the significance. The consideration of the sign of the Hall coefficient lets the correlation approach zero (#5). However, the enlarged data set has only slight impact on the correlation to x (#6). Logarithmizing Eq. (19) leads to a linear model with a slope of $b = \frac{1}{2}$ and a positive intercept a containing the other quantities. Regression attempts based on it are listed in Table III, where σ_i is here the corresponding standard error of the two parameters.

The influence of the error δn_{eff} can be seen in comparison of #1 and #2, where #1 has been willfully ascribed an error of 20% by the authors and #2 adopts a more realistic value of 10%. The resulting slopes definitely stay behind the necessary

TABLE III. Regressions on $\ln n_{\text{eff}} \mapsto \ln U_e$.

Number[a]	a	b	σ_a	σ_b	χ^2	Q value
1	5.87	0.41	0.03	0.04	110.6	1.99×10^{-13}
2[b]	5.91	0.34	0.03	0.04	136.0	5.01×10^{-18}
3[c]	6.03	−0.02	0.02	0.01	385.3	1.50×10^{-56}

[a]Data of Ref. [14], Table 1.
[b]$\delta n_{\text{eff}} = 10\%$.
[c]Including data from Refs. [25,26], Table 1 and n_{eff} for the omitted elements.

value of 1/2. Making worse the goodness of the fit (the Q value) remains tiny. Conventionally, if the goodness is smaller than 10^{-3} the model is considered incorrect or the errors are still roughly underestimated. Here (#3) the inclusion of the temperature-dependent data [25,26], Table 1 and n_{eff} for the omitted elements In, Sn, Sb, Pb, and Bi in the calculations leads to a slope close to zero and a goodness of fit disqualifying the linear model. The value of the Hall coefficient of Pd was doubted in Ref. [14]) and replaced by their own measurement with minor impact. So in both instances, correlation and regression, the explanation by the Debye hypothesis is ruled out. The disaffirmation of the Debye hypothesis on the basis of the correlation tests alone might be disputable, together with the other aforementioned points it becomes decrepit. The density hypothesis as an alternative clearly could not be falsified. Complemented by the preceding argumentation and the physicochemical effects as described in Ref. [16] Secs. 4 and 6) and Sec. III the deuteron density dynamics provide the explanation for the alleged screening results. Thus the assumptions for reactions with heavier nuclei and radioactive decay are refuted as well with the consequence that any experimental evidence offered for them needs to come under scrutiny.

B. Experiments with heavier nuclei

As a consequence of the conclusions of Sec. V A the erratic high screening findings of the other groups cannot really serve as a confirmation of our results. Therefore the experiments on Li target nuclei achieve special significance as a independent reassurance for the overall effect of the enhancement of nuclear reactions in metallic environments. With regard to the reliability the most outstanding result discussed here is from the experimental on $d + \text{Li}$ in binary alloys with Pd and Au [19]. The α yield from the reactions at ^{6,7}Li (with natural abundances of 7.42% ^{6}Li and 92.58% ^{7}Li) in both alloys was observed normalized to the yield at 75 keV in complete analogy to the procedure for the d+d reaction [9,10] and set in relation to LiF targets. The inferred screening energies are (1500 ± 310) eV for PdLi_x and (60 ± 150) eV for AuLi_x, where x was initially at 5%–10% for the alloys. The screening energy for PdLi_x is therewith one order of magnitude higher than our value of (190 ± 50) eV for ^{6}LiF, which is in agreement with the simple theory [50]. The latter screening energy is substantially smaller than the (380 ± 250) eV from Ref. [51]. This is because a significant share of the increase of the observed S factor toward low energies is caused by a 2^+subthreshold resonance at $E_x(^8\text{Be}) = 22.2$ MeV, which needs to be included in the data analysis by sophisticated nuclear reaction theoretical calculations [50,52]. The advantage of this experiment on Li targets over deuterium is that the small hydrogen atoms have a mobility in metals that is several orders of magnitude greater than other atom species. Thus, unlike the auto implanted deuterium targets there is no such fatal target atom density dynamics possible as in Ref. [[16], Figs. 13(a)–13(d)] [Figs. 6(b) and 6(c)]. The, also here inevitable, oxidation process will only decrease—but not completely supplant—the Li fraction in the surface layers. This together with the higher sputtering yield for light atoms explains the observed asymptotic bisection of the yield with the ion dose [19], Fig. 2 at the monitor energy of 75 keV. Both lead to an inhomogeneous depth distribution of the Li target atoms with a lower Li fraction at the surface because of the higher beam energies ($\geqslant$30 keV) with lower impact. So this time the observed enhancement can be regarded as a lower limit, too, whereas the inferred value of the screening energy needs to be corrected for the influence of the subthreshold resonance and the same questions regarding the screening energy calculation of the authors apply as in the case of deuterium. The low value for AuLi_x is so far in conformity with the negative findings for the d+d reaction in Au [9,10,12,13]. A similar experiment [20] was later performed by using the proton-induced reactions on ^{6,7}Li in an environment of Li_2WO_4, Li metal, and PdLi_x ($x = 1\%, 0.01\%$). The results for the screening energies of the reaction $^7\text{Li}(p,\alpha)\alpha$ are (185 ± 150) eV for Li_2WO_4, (1280 ± 60) eV for the metal, and (3790 ± 330) eV for $\text{PdLi}_{1\%}$, which were obtained by using standard procedures [Eqs. (14) and [15]] [11,46]. The results for $\text{LiPd}_{0.01\%}$ and the reaction $^6\text{Li}(p,\alpha)^3\text{He}$ agree within 1σ. In a microscopic view it is universally valid that the screening effect depends on the impact of the electronic configuration of the environment on the Coulomb barrier of the entrance channel only (e.g., Refs. [53,54]); that is, the pure Coulomb energy is modified by a Yukawa factor for simplicity, $W(r) = \frac{1}{4\pi\varepsilon_0}\frac{Z_p Z_t e^2}{r} e^{-\frac{r}{\lambda_A}}$, with λ_A being the screening length. As such the inferred screening energy is merely the second term in a Taylor expansion of $W(r)$ (i.e., $U_e = \frac{1}{4\pi\varepsilon_0}\frac{Z_p Z_t e^2}{\lambda_A}$) and a coarse mathematical parametrization in the simple model [2] [Eq. (7)] [16, Eq. (20)]. The screening modification of the Coulomb potential only acts as if the projectile gained U_e. So there is no "acceleration mechanism" in reality and one must neither decompose the screening effect nor transfer the result of one environment to another as in Ref. [20], where the "atomic" screening energy for $^7\text{Li} \rightarrow \text{H}_2$ is used as a linear addend in the screening energy for $p \rightarrow$ (Li metal or PdLi_x). Consequently, the screening energy is independent of the isotopes in the reaction and should be equal for ^{1,2}H+^{6,7}Li in Refs. [19] and [20]. However, there are two discrepancies between Refs. [20] and [19]: First, the screening energy for PdLi_x of Ref. [20] is more than twice as high as that of Ref. [19]. But four of the seven data points lay offside the fitted curve and only the fit error is given for U_e [20], Figs. 1 and 2). Second, in Ref. [20] it was asserted that the yield remained stable to better than 10% whereas in Ref. [19] a bisection of the yield at 6 C was observed, which is plausible from irradiation effects. Both discrepancies can be explained by the

different target fabrication techniques. In Ref. [19] Pd and Li are made into an alloy by arc melting whereas in Ref. [20] Li was inserted in a Pd disk in a plasma discharge. The latter is prone to depth inhomogeneities. This was verified by a nuclear reaction analysis (NRA) of the target by using the $E_\alpha = 958$ keV resonance with a width of $\Gamma = 4$ keV in the reaction $^7\mathrm{Li}(\alpha,\gamma)^{11}\mathrm{B}$, yielding the ascertainment of a homogeneous depth distribution [20]. However, the depth resolution of this method is limited by the energy uncertainty and spread of the beam and the width of the resonance. The most prominent example of the NRA is the $E_\mathrm{N} = 6.385$ MeV resonance with a width of $\Gamma = 1.8$ keV in the reaction $^1\mathrm{H}(^{15}\mathrm{N},\alpha\gamma)^{12}\mathrm{C}$ for the investigation of hydrogen distributions. It has a minimal resolution ranging from 5 to 15 nm [55]. So the resolution of the Li NRA is worse given a 2.2 times higher width of the resonance. Since most of the yield is contributed by the topmost atomic layers here as well [[16], Sec. 4.3, Fig. 10(d)], an enhanced Li content below the NRA resolution at the surface would explain the more than two times higher screening energy and the much lower decrease of the yield with the ion dose. The high screening value for PdLi_x was regarded as a confirmation for the Debye model. If this were true the measurements for AuLi_x [19] should also have yielded a high value and not one close to zero, since the $d+d$ screening energy for Au of Ref. [14] was about 280 eV, which differed from the results of Refs. [9,10,12,13] and our observation.

The theoretical model of the electron screening presented in Sec. IV B predicts different screening energies for different target material environments. In the case of an insulator the electron screening should reach a value of 190 eV, which results only from the gain of the electron binding energies. For metallic environments the contribution coming from free electrons has to be included additionally. Owing to different electron densities for Pd ($r_S = 1.4$) and Li ($r_S = 3.4$) the free electron contributions to the screening energy are equal to 660 and 420 eV, respectively. Thus, we finally expect total screening energies of 190 eV for an insulating target material, 610 eV for metallic lithium targets, and 850 eV for the PdLi_x alloy. Experimental results, despite large uncertainties, confirm different electron screening energies for insulating and metallic materials with various electron densities.

In extending this thread, a first effort was undertaken in Ref. [21] to study the environmental influence for heavy nuclei using the (p,n) reaction on $^{50}\mathrm{V}$ and $^{176}\mathrm{Lu}$ nuclei in an oxide, as pure metal, and as an alloy with Pd in the energy range 0.75–1.5 MeV. Because of insufficient cross-section data the screening energies were obtained by comparison with the metal oxides VO_2 and $\mathrm{Lu}_2\mathrm{O}_3$. The inferred screening energies are (27 ± 9) keV and (33 ± 11) keV for V and $\mathrm{PdV}_{10\%}$ and (32 ± 2) keV and (33 ± 2) keV for Lu and $\mathrm{PdLu}_{10\%}$. The comparison was made by taking the ratio of the yields between the metal and the oxide, designated as insulator,

$$R(E_p) = \frac{Y_m(E)}{Y_i(E)} = \frac{\int_0^{E_p} \delta_n(E)\varepsilon_m^{-1}(E)\sigma_m(E)dE}{\int_0^{E_p} \delta_n(E)\varepsilon_i^{-1}(E)\sigma_i(E)dE}, \qquad (20)$$

where δ_n is the efficiency of the neutron detector. It is now assumed that the ratio of the stopping cross sections between the two materials can be expressed by an energy-independent constant $\alpha = \varepsilon_i(E)/\varepsilon_m(E)$, which is mathematically doubtful considering Bragg's rule [56]. So the following substitutions where made: $\varepsilon_m(E) = \alpha^{-1}\varepsilon_i(E)$ and $\sigma_m(E) = f(E)\sigma_i(E)$ with the enhancement factor f as in Eq. (7) with the presupposition of a constant S. The ratio of the integrals is further simplified by the energy differentiation of the yields by using the effective energy as in Eqs. (14) and (15) [11, Eq. (5), (7), and (8)] to arrive at $R(E_p) = \alpha f(E_\mathrm{eff})$. The screening energy together with α resulted from a fit to the yield ratios. This procedure was, however, only applied to V. The screening energies for Lu were gathered from the shift of the Lewis peak along the energy axis between the different targets originating from a narrow resonance close to $E_p = 0.8$ MeV [21], Fig. 3. The Lewis effect comes from the discrete energy loss of the projectiles in the target [57]. This energy shift was indeed erroneously interpreted as the screening energy. As already pointed out, the screening effect is merely a modification of the Coulomb barrier and implies no real energy shift. So this shift cannot originate from the screening effect. Thus, it is probable that the energy shift is caused by target properties. The oxide targets, being the normalization standard, are made by pressing a metal oxide powder into a cylindrical hole of a Cu disk. It is well known from powder metallurgy and silicate technology that pressing a powder like this is insufficient to remove the hollow spaces between the powder particles unless a sintering step is performed. So the used metal oxide targets contain hollow spaces with a size of the same order of magnitude as the powder particles. Consequently, the stopping of MeV protons is heavily altered in comparison to a monolithic metal oxide ceramic and different in its mathematical description to that of Ref. [30]. We observed effects of porous targets on the stopping [38], Fig. 2. So the shift of the Lewis peak can be explained by the differences of the stopping between the porous metal oxide target and the metal targets. Additionally, it is well known that the position and form of the Lewis peak depends very critically on the composition, homogeneity, and contamination of the target (see Refs. [57–59]) and also Ref. [46]). This in turn casts serious doubts on the results for V. A critical point of the data analysis [Eq. (20)] is the presupposition that the ratio of the stopping cross sections of the metal oxide and the metal is a constant over the energy. This is inappropriate for the porous target and can lead to a misinterpretation of the data. The conspicuously high errors of the screening and α values from the fit—about 33%, making the effect compatible with zero within 3σ—are a strong indication for a high correlation between the two fit parameters showing the improperness of the fit model. The covariance matrix of the fit parameters could have given information about this.

From the theoretical point of view the large screening energies obtained for the $d+d$ reactions at energies below 20 keV cannot be used for the estimation of the screening energies in this case since the proton energy is much higher and does not fulfill the adiabatic approximation. Since the surrounding electrons are much slower than the protons, the resulting screening energy obeys rather assumptions of the sudden approximation and thus should be of order of a few keV, contrasting with the statements in Refs. [20,21].

TABLE IV. Decay of radionuclides embedded in host metals.

Ref.	Nuclide	Decay mode	Host	Prediction (%)	Measurement (%)
[22]	^{22}Na	90% β^+	Pd	11	(1.2 ± 0.2)
[61]	^{198}Au	100% β^-	Au	-34	(-4.0 ± 0.7)
[62]	^{210}Po	100% α	Cu	3300	(6.3 ± 1.4)

C. Radioactive decay of embedded nuclei

As the electron screening enhances the cross section at low impact energies, a similar effect can be expected for the radioactive decay. However, since the energies of the decay products are fixed by the Q value, only a few nuclei with lowest energy emitters are candidates for a measurable change in the lifetime. In general, for positive charged ejectiles (α and β^+ decay), screening reduces the Coulomb barrier and therefore enhances the decay rate whereas the opposite is true for β^- decay. As recently pointed out by Zinner [60] the effect of a changed Coulomb barrier is partially canceled by a modified Q value that stems from the extension of the screened potential into the inner part of the nucleus. For heavy nuclei the effect can still be strong as the screening potential scales approximately with the product of the charge number of the end nuclei.

Recently, based on an extrapolation of the Debye-Hückel electron screening model to low temperatures, it has been suggested that half-lives of radioactive isotopes may change by orders of magnitude if they are embedded in a metal lattice and cooled to cryogenic temperatures [21,23,25,27,28].[9] In support of these predictions, a series of measurements has been published, the results of which are listed in the Table IV, together with the half-life changes predicted by the Debye-Hückel model.

The striking disagreement with the predictions have been attributed to an oxygen layer buildup on the metal surface leading to an insufficient implantation of the radioisotope.[10]

A recently published measurement [63,64] where ^{22}Na was activated in Al (and therefore deeply implanted) clearly shows a zero effect on a level of 0.04%, again in striking disagreement to the results in Ref. [22] with a reported lifetime change of (1.2 ± 0.2)% (see Table IV). No description pf how the data have been analyzed has been given in Ref. [22]. If the 511-keV annihilation line has been included in the analysis, the results are certainly not correct (see Ref. [66]). For the α decay, even the observed 6% [62] change is surprising as embedding radioactive nuclei in metals and cooling the samples to cryogenic temperatures has been a routine procedure in low temperature nuclear orientation (LTNO) experiments for several decades.[11] Stone *et al.* [67] studied in detail the expected effect with respect to α decay on complete decay chains starting with ^{224}Rn, ^{225}Ra, and ^{227}Ac and compared it with available LTNO data. None of those data indicate any change of the lifetime of any of the nuclei involved when they are implanted into iron, neither at room temperature nor when cooled to 20 mK. The same applies for β active nuclei in multiple host metals (see Ref. [67] and references therein). The precision of these measurements is typically 1% and less. Another follow-up measurement performed at ISOLDE/CERN [68] focused on a possible change of the ^{221}Fr (α decay) half-life when embedded in a metal and an insulator; there is also no clear effect (50% error) on a level of 0.3%. Severijns *et al.* [69] investigated the α decay of ^{253}Es in Fe between 4 K and 50 mK and could not observe any effect on a level of 2%. Finally, the β^- decay of ^{198}Au embedded in Au and Al-Au has been measured independently by three different groups [64,70,71], and no lifetime change could be observed on a subpercent level when the sample was cooled to $\approx$ 10 K. The latest result [64] was measured with a 30 times better accuracy but the same conditions as in Ref. [61].

In conclusion, all the follow-up measurements are in agreement with the theoretical expectations presented already in Sec. IV B. The Debye-Hückel screening can be applied only for temperatures higher than the Fermi temperature (typically 10^5 K), far above the evaporation temperature of metals. For lower temperatures one should not observe any temperature dependence of the screening energy.

However, another effect can be expected [41]: a change of the lifetime by just embedding the unstable nuclei into a metal, but this requires an absolute measurement of the lifetime and therefore much more experimental effort. A reanalysis of past lifetime measurement data with respect to the chemical composition could also reveal such a dependence. For instance, the lifetime of ^{238}U has been determined with electroplated samples (metallic uranium), U_3O_8, and other compounds (see Refs. [72,73]). Although the measurements scatter by 1%–2%, no systematic enhancement of the decay rate can be seen for the metallic uranium. As can be seen from the aforementioned CERN measurement [68] the effect will be small anyway even for high screening values but any evidence would be a great contribution to a better understanding of the screening mechanism from a very different approach.

VI. CONCLUSION

We presented some new experimental electron screening energies for $d+d$ reactions taking place in different target material environments. We applied a differential data analysis method that gains the maximum information from the raw data. The method is independent of the unprecise stopping power coefficients and the actual absolute value of the deuteron number density in the targets. It enables the on-line monitoring of the deuteron densities and the observation of short-time deuteron density profile changes. Thus, it allows for the recognition and rejection of measurements with unwanted shifts in the density depth distribution profile. Therefore, it adequately considers the special situation of potentially highly mobile hydrogen in solid states where neither a homogeneous nor a stable density distribution can be presupposed any

[9] This effect has also been proposed as a new method of disposing of radioactive waste from nuclear power plants [23,27,28].

[10] Publications concerning a change in ^{7}Be lifetime are not taken into account as ^{7}Be decays via capture of s-wave electrons, which is not influenced by electron screening.

[11] It should be noted that polonium is known to be very movable in metals [65]; therefore an alteration of the measured activity could be due to changes in the polonium distribution.

longer. The problem of the density dynamics is entangled with the effects from the actual target composition; that is, the undesirable density profile changes occur in targets with low hydrogen binding ability, like many of the transition metals, at elevated temperatures, and with heterogeneous targets with metal oxide or carbon layers or different (relatively) thin metal layers. The formation of metal oxide layers is inevitable in common high vacuum systems used in experimental nuclear physics but the other unpropitious environments were produced deliberately. Thorough investigation of the contamination layer formation showed their momentousness and together with the differential analysis method assured that our screening energy values ranging between 190 and 320 eV represent lower limits. In addition the alteration of the inferred screening energies caused by layer formation under beam irradiation depends on many parameters. Logically it makes no sense to measure larger portions of the periodic table since any observed material dependence results from differences in the chemical reactivity and related physicochemical properties for the contamination layer formation, unless this problem is reliably solved. Note that our high screening energy results were achieved at high densities in the proximity of the chemical stoichiometric ratio clearly without evidence for short-time density profile shifts whereas the high screening results of the other groups were exclusively attained at low densities, yielded from the customary analysis of the total yields of the measurements, which is ignorant of the concurrent density dynamics. The target diagnosis methods are unusable because of their too coarse resolution and off-line application. So the inferred screening energies are conjecturally simulated by the density dynamics. Using explorative statistics on the data sets including the temperature measurements sustains this explanation but the Debye-Hückel hypothesis is clearly falsified. It is likewise falsified from the theoretical side since calculations performed within an improved dielectric function theory predict only a weak material dependence of U_e on the valence electron density. The quantitative scale of the phenomenon is not yet understood, since our analytical model still fails to describe the values by at least a factor of 2. So further unidentified effects play a role. Consequently, any conclusion based on the alleged material dependence of the inferred screening energies is premature. For that purpose the precise determination of the screening energies is required, and this is only feasible in an ultra high vacuum system with pressures well below 10^{-10} hPa, where only hydrogen and noble gases are in the residual gas, and equipped with in situ target diagnosis techniques. We performed the first measurements under UHV conditions, whose results confirm the previous measurements and the framework of surface physics and chemical effects [74].

Nuclear reactions with heavier nuclei embedded in metallic environments gave evidence for an alike enhanced screening effect. However, there are analogous problems. The results for deuterated metals with ^{3}He projectiles are contradictory, most probably because of deuteron dynamics. The data for Li nuclei are partially conflicting between the Tohoku and the Bochum groups, who used different target preparation techniques, and can be attributed to inhomogeneous densities and inadequate diagnosis techniques as well. The results, however, confirm theoretical predictions based on the dielectric function theory concerning the free electron density of the target material. The screening energy data for the heavier nuclei V and Lu were obtained from a comparison between a metal and a metal oxide powder target, in which the hollow spaces in the powder and its strong influences on beam stopping have been ignored, thus disabling any conclusions.

As discussed, the predictions of the Debye-Hückel hypothesis given by the Bochum group for the temperature dependence of the radioactive decay of embedded nuclei could not be verified by their own experiments; the measured values are orders of magnitude below their predictions. Moreover, their experimental results contradict those of all other experiments, in particular the LTNO measurements of the past 30 years. A material dependence is conceivable, though it would be a small effect, for otherwise it would have already been discovered given that nuclei of importance for nuclear technology have been investigated in multiple chemical compounds including pure metals for decades.

[1] E. E. Salpeter, Aust. J. Phys. **7**, 373 (1954).
[2] H. J. Assenbaum, K. Langanke, and C. Rolfs, Z. Phys. A **327**, 461 (1987).
[3] C. Rolfs and E. Somorjai, Nucl. Instrum. Methods B **99**, 297 (1995).
[4] K. Czerski, A. Huke, P. Heide, M. Hoeft, and G. Ruprecht, in *Nuclei in the Cosmos V, Proceedings of the International Symposium on Nuclear Astrophysics*, edited by N. Prantzos and S. Harissopulos (Editions Frontières, Volos, Greece, 1998), p. 152.
[5] K. Czerski, A. Huke, A. Biller, P. Heide, M. Hoeft, and G. Ruprecht, Europhys. Lett. **54**, 449 (2001).
[6] A. Huke, Ph.D. thesis, Technische Universität Berlin, 2002, http://edocs.tu-berlin.de/diss/2002/huke_armin.htm.
[7] U. Greife, F. Gorris, M. Junker, C. Rolfs, and D. Zahnow, Z. Phys. A **351**, 107 (1995).
[8] S. Ichimaru, Rev. Mod. Phys. **65**, 252 (1993).
[9] H. Yuki, J. Kasagi, A. G. Lipson, T. Ohtsuki, T. Baba, T. Noda, B. F. Lyakhov, and N. Asami, JETP Lett. **68**, 823 (1998).
[10] J. Kasagi, H. Yuki, T. Baba, T. Noda, T. Ohtsuki, and A. G. Lipson, J. Phys. Soc. Jpn. **71**, 2881 (2002).
[11] F. Raiola *et al*., Eur. Phys. J. A **13**, 377 (2002).
[12] F. Raiola *et al*., Phys. Lett. **B547**, 193 (2002).
[13] C. Bonomo *et al*., Nucl. Phys. **A719**, 37c (2003).
[14] F. Raiola *et al*., Eur. Phys. J. A **19**, 283 (2004).
[15] K. Czerski, A. Huke, P. Heide, and G. Ruprecht, Eur. Phys. J. A **27**, 83 (2006).
[16] A. Huke, K. Czerski, and P. Heide, Nucl. Instrum. Methods B **256**, 599 (2007).
[17] A. Huke, K. Czerski, S. M. Chun, A. Biller, and P. Heide, Eur. Phys. J. A **35**, 243 (2008).
[18] K. Czerski, A. Huke, P. Heide, and G. Ruprecht, Europhys. Lett. **68**, 363 (2004).
[19] J. Kasagi, H. Yuki, T. Baba, T. Noda, J. Taguchi, M. Shimokawa, and W. Galster, J. Phys. Soc. Jpn. **73**, 608 (2004).

[20] J. Cruz *et al.*, Phys. Lett. **B624**, 181 (2005).
[21] K. U. Kettner, H. W. Becker, F. Strieder, and C. Rolfs, J. Phys. G **32**, 489 (2006).
[22] B. Limata *et al.*, Eur. Phys. J. A **28**, 251 (2006).
[23] C. Rolfs, Nuclear Physics News **16**, 9 (2006).
[24] G. Ruprecht, L. Buchmann, D. Hutcheon, D. Ottewell, C. Ruiz, P. Walden, C. Vockenhuber, and K. Czerski, in *Nuclei in the Cosmos IX*, *Proceedings of the International Symposium on Nuclear Astrophysics*, Vol. PoS(NIC-IX)171 (2006).
[25] F. Raiola *et al.*, J. Phys. G **31**, 1141 (2005).
[26] F. Raiola *et al.*, Eur. Phys. J. A **27**, 79 (2006).
[27] P. Ball, Nature News (2006).
[28] H. Muir, New Scientist **2574**, 36 (2006).
[29] C. Rolfs, as quoted in Frankfurter Allg. Ztg. 08-13 (2006).
[30] H. Anderson and J. F. Ziegler, *The Stopping and Ranges of Ions in Matter*, Vol. 3 (Pergamon Press, New York, 1977).
[31] R. E. Brown and N. Jarmie, Phys. Rev. C **41**, 1391 (1990).
[32] S. P. Møller, A. Csete, T. Ichioka, H. Knudsen, U. I. Uggerhøj, and H. H. Andersen, Phys. Rev. Lett. **93**, 042502 (2004).
[33] W. M. Mueller, J. P. Blackledge, and G. G. Libowitz, eds. *Metal Hydrides* (Academic Press, New York, London, 1968).
[34] W. Ensinger, Nucl. Instrum. Methods B, 796 (1997).
[35] A. Zangwill, *Physics at Surfaces* (Cambridge University Press, Cambridge, 1988).
[36] D. Kamke, *Handbuch der Physik* (Springer Verlag, Berlin, 1956), Vol. XXXIII, Chap. 1.
[37] W. T. Hering, *Angewandte Kernphysik* (Teubner, Stuttgart, Leipzig, 1999).
[38] A. Huke, K. Czerski, T. Dorsch, A. Biller, P. Heide, and G. Ruprecht, Eur. Phys. J. A **27**, 187 (2006).
[39] G. Grosso and G. P. Parravicini, *Solid State Physics* (Academic Press, New York, 2000).
[40] J. F. Ziegler, J. P. Biersack, and U. Littmark, *The Stopping and Ranges of Ions in Matter* (Pergamon Press, New York, 1985).
[41] K. Czerski, P. Heide, A. Huke, L. Martin, and G. Ruprecht, in *Nuclei in the Cosmos IX*, *Proceedings of the International Symposium on Nuclear Astrophysics*, Vol. PoS(NIC-IX)044 (2006).
[42] A. F. Lifschitz and N. R. Arista, Phys. Rev. A **57**, 200 (1998).
[43] J. Roth, R. Behrisch, W. Möller, and W. Ottenberger, Nucl. Fusion **30**, 441 (1990).
[44] H. S. Bosch and G. M. Hale, Nucl. Fusion **32**, 611 (1992).
[45] T. S. Wang, Z. Yang, H. Yunemura, A. Nakagawa, H. Y. Lv, J. Y. Chen, S. J. Liu, and J. Kasagi, J. Phys. G **34**, 2255 (2007).
[46] C. E. Rolfs and W. S. Rodney, *Cauldrons in the Cosmos*, Theoretical Astrophysics (University of Chicago Press, Chicago and London, 1988).
[47] A. Huke, K. Czerski, and P. Heide, Nucl. Phys. **A719**, 279c (2003).
[48] W. Stahel, *Statistische Datenanalyse* (Vieweg, Braunschweig, Wiesbaden, 2002), 4th ed.
[49] C. M. Hurd, *The Hall Effect in Metals and Alloys* (Plenum, New York, 1972).
[50] K. Czerski, A. Huke, H. Bucka, P. Heide, G. Ruprecht, and B. Unrau, Phys. Rev. C **55**, 1517 (1997).
[51] S. Engstler, G. Raimann, C. Angulo, U. Greife, C. Rolfs, U. Schröder, E. Somorjai, B. Kirch, and K. Langanke, Phys. Lett. **B279**, 20 (1992).
[52] G. Ruprecht, K. Czerski, D. Bemmerer, M. Hoeft, and P. Heide, Phys. Rev. C **70**, 025803 (2004).
[53] T. D. Shoppa, S. E. Koonin, K. Langanke, and R. Seki, Phys. Rev. C **48**, 837 (1993).
[54] T. D. Shoppa, M. Jeng, S. E. Koonin, K. Langanke, and R. Seki, Nucl. Phys. **A605**, 387 (1996).
[55] G. Schatz and A. Weidinger, *Nukleare Festkörperphysik* (Teubner, Stuttgart, 1992), 2nd ed.
[56] R. Bragg, Phil. Mag. 318 (1905).
[57] H. W. Lewis, Phys. Rev. **125**, 937 (1962).
[58] W. L. Walters, D. G. Costello, J. G. Skofronick, D. W. Palmer, W. E. Kane, and R. G. Herb, Phys. Rev. Lett. **7**, 284 (1961).
[59] J. M. Donhowe, J. A. Ferry, W. G. Monrad, and R. G. Herb, Nucl. Phys. **A102**, 383 (1967).
[60] N. T. Zinner, Nucl. Phys. **A781**, 81 (2007).
[61] T. Spillane *et al.*, Eur. Phys. J. A **31**, 203 (2007).
[62] F. Raiola *et al.*, Eur. Phys. J. A **32**, 51 (2007).
[63] G. Ruprecht, C. Vockenhuber, C. Ruiz, L. Buchmann, J. Pearson, D. Ottewell, K. Czerski, and A. Huke, J. Phys. G: Nucl. Part. Phys. **35**, 014017 (2008).
[64] G. Ruprecht, C. Vockenhuber, L. Buchmann, R. Woods, C. Ruiz, S. Lapi, and D. Bemmerer, Phys. Rev. C **77**, 065502 (2008).
[65] A. Zastawny *et al.*, Appl. Radiat. Isotopes **43**, 1147 (1992).
[66] K. F. Canter, A. P. Mills, and S. Berko, Phys. Rev. Lett. **33**, 7 (1974).
[67] N. J. Stone, J. R. Stone, M. Lindroos, P. Richards, M. Veskovic, and D. A. Williams, Nucl. Phys. **A793**, 1 (2006).
[68] H. B. Jeppesen, J. Byskov-Nielsen, P. Wright, J. G. Correia, L. M. Fraile, H. O. U. Fynbo, K. Johnston, and K. Riisager, Eur. Phys. J. A **32**, 31 (2007).
[69] N. Severijns *et al.*, Phys. Rev. C **76**, 024304 (2007).
[70] J. R. Goodwin, V. V. Golovko, V. E. Iacob, and J. C. Hardy, Eur. Phys. J. A **34**, 271 (2007).
[71] V. Kumar, M. Hass, Y. Nir-El, G. Haquin, and Z. Yungreiss, Phys. Rev. C **77**, 051304 (2008).
[72] R. Schön, G. Winkler, and W. Kutschera, Appl. Radiat. Isotopes **60**, 263 (2004).
[73] A. H. Jaffey, K. F. Flynn, L. E. Glendenin, W. C. Bentley, and A. M. Essling, Phys. Rev. C **4**, 1889 (1971).
[74] K. Czerski, A. Huke, L. Martin, N. Targosz, D. Blauth, A. Górska, P. Heide, and H. Winter, J. Phys. G **35**, 014012 (2008).